OPEN ACCESS Freely available online

PLoS one

Correlation Index-Based Responsible-Enzyme Gene Screening (CIRES), a Novel DNA Microarray-Based Method for Enzyme Gene Involved in Glycan Biosynthesis

Harumi Yamamoto[1,4], Hiromu Takematsu[1,5]*, Reiko Fujinawa[4], Yuko Naito[1,5], Yasushi Okuno[2], Gozoh Tsujimoto[3], Akemi Suzuki[4], Yasunori Kozutsumi[1,4,5]

1 Laboratory of Membrane Biochemistry and Biophysics, Graduate School of Biostudies, Kyoto University, Sakyo, Kyoto, Japan, 2 Department of PharmacoInformatics, Graduate School of Pharmaceutical Sciences, Kyoto University, Sakyo, Kyoto, Japan, 3 Department of Genomic Drug Discovery, Graduate School of Pharmaceutical Sciences, Kyoto University, Sakyo, Kyoto, Japan, 4 Supra-Biomolecular System Research Group, RIKEN Frontier Research System, RIKEN, Wako, Saitama, Japan, 5 Core Research for Evolutional Science and Technology (CREST), Japan Science and Technology Corporation (JST), Kawaguchi, Saitama, Japan

Background. **Glycan biosynthesis occurs though a multi-step process that requires a variety of enzymes ranging from glycosyltransferases to those involved in cytosolic sugar metabolism. In many cases, glycan biosynthesis follows a glycan-specific, linear pathway. As glycosyltransferases are generally regulated at the level of transcription, assessing the overall transcriptional profile for glycan biosynthesis genes seems warranted. However, a systematic approach for assessing the correlation between glycan expression and glycan-related gene expression has not been reported previously.** ***Methodology.*** **To facilitate genetic analysis of glycan biosynthesis, we sought to correlate the expression of genes involved in cell-surface glycan formation with the expression of the glycans, as detected by glycan-recognizing probes. We performed cross-sample comparisons of gene expression profiles using a newly developed, glycan-focused cDNA microarray. Cell-surface glycan expression profiles were obtained using flow cytometry of cells stained with plant lectins. Pearson's correlation coefficients were calculated for these profiles and were used to identify enzyme genes correlated with glycan biosynthesis.** ***Conclusions.*** **This method, designated correlation index-based responsible-enzyme gene screening (CIRES), successfully identified genes already known to be involved in the biosynthesis of certain glycans. Our evaluation of CIRES indicates that it is useful for identifying genes involved in the biosynthesis of glycan chains that can be probed with lectins using flow cytometry.**

Citation: Yamamoto H, Takematsu H, Fujinawa R, Naito Y, Okuno Y, et al (2007) Correlation Index-Based Responsible-Enzyme Gene Screening (CIRES), a Novel DNA Microarray-Based Method for Enzyme Gene Involved in Glycan Biosynthesis. PLoS ONE 2(11): e1232. doi:10.1371/journal.pone.0001232

INTRODUCTION

The biosynthesis of glycan chains is a multi-step process. First, free sugars are biosynthesized by sugar-specific metabolic pathways. Then, these sugar molecules are further metabolized to nucleotide sugars, which serve as donors for glycosyltransferases [1]. Specific transporters move the nucleotide sugars to the endoplasmic reticulum (ER) or Golgi apparatus [2], where they are utilized by glycosyltransferases for the tandem addition of sugars to the termini of nascent glycan chains in a sugar- and linkage-specific manner [3]. This lengthy glycosylation process requires a great number of different enzymes operating at various levels of synthesis.

Thus far, more than 300 enzymes and transporter genes have been reported to be involved in the metabolism and biosynthesis of different glycans in diverse cell types and at various stages. Each glycan structure has its own specific biosynthetic pathway. The introduction of cloning expression methodology [4,5] has led to the successful cloning of a glycosyltransferase and to the demonstration that overexpression of a glycosyltransferase cDNA clone can confer the capability of glycan biosynthesis in over-expressing cells [6]. This mechanism is in contrast to that used by protein kinases, which also act via pathway-like processes but are often positively or negatively regulated by phosphorylation.

DNA microarray technology is very powerful because it can simultaneously detect changes in the expression levels of a large number of genes. In the field of glycobiology, extensive efforts have been made to identify the genes involved in glycan biosynthesis, and many have been shown to encode glycosyltransferases of the ER or Golgi apparatus. Many of these genes have been cloned, including those encoding large enzyme families [7]. Given the important role of gene transcription in the regulation of glycan biosynthesis, a glycan-focused cDNA microarray was developed to obtain the transcriptome of glycan-related genes [8,9]. As the presentation of glycomic information on a cell surface is likely to be regulated at the level of transcription of the enzymes in biosynthetic pathways, a glycan-focused DNA microarray may prove useful in elucidating glycan expression [8,10].

In the present study, we analyzed the glycan-related gene expression profiles for possible correlations with cellular glycan expression profiles in a cross-sample manner, using Pearson's

Academic Editor: Stefan Wölfl, Universität Heidelberg, Germany

Received March 19, 2007; **Accepted** November 4, 2007; **Published** November 28, 2007

Funding: This work was supported by CREST, JST, a grant-in-aid program from the Ministry of Education, Culture, Sports, Science and Technology of Japan, and by RIKEN.

Competing Interests: The authors have declared that no competing interests exist.

* **To whom correspondence should be addressed.** E-mail: htakema@pharm.kyoto-u.ac.jp

correlation coefficient. This analysis successfully identified specific genes encoding regulatory enzymes for the biosynthesis of specific glycans, from among the candidate genes of the glycan biosynthesis pathways. We designated this method correlation index-based responsible-enzyme gene screening, or CIRES (Figure 1).

RESULTS

Glycan-related gene-expression profiling using cDNA microarrays

The rat monoclonal antibody GL7 specifically stains germinal center B cells upon T cell-dependent antigen immunization. We recently demonstrated that GL7 recognizes the glycan Neu5Acα_{2-6}-Galβ_{1-4}-GlcNAc-R and that the sialyltransferase gene *ST6GAL1* is responsible for the biosynthesis of the glycan epitope recognized by GL7 [11]. By analyzing the correlation between the expression profiles for sialic acid (Sia) metabolism-related genes and the expression profiles for the GL7 epitope in a cross-sample manner, we showed that this type of correlation analysis was useful in screening for genes involved in the biosynthesis of the glycan epitope. In the present study, we further developed this systematic methodology by analyzing the correlations for cross-sample comparisons between the expression profiles for glycan-related genes and the expression profiles for various glycans, as determined by specific lectin binding (Figure 1).

The glycan-related gene expression profiles were obtained using total RNA isolated from six human B-cell lines cultured under optimal conditions, and cross-sample comparisons of these profiles were made in relation to a commercially available universal reference RNA consisting of a mixture of polyA(+) RNA from various organs. The gene expression profiles were determined as a ratio of the gene expression level to the universal reference cDNA expression level on the glycan-focused microarray ([11]; the complete relative gene expression profiles are shown in Table S1). Thus, the glycan-related gene expression profiles are expressed as the ratio of the gene expression signal at each spot on the microarray relative to the reference RNA signal.

After staining the cells with various anti-glycan probes (lectins) of known specificity, we determined the glycan expression profiles using flow cytometry. For each cell line, the transcriptional profile of glycan-related genes was used for cross-sample correlation analysis with the glycan expression profile.

Cell-surface glycan expression profiling using flow cytometric detection of lectin staining

Cell-surface glycan expression has been extensively studied using plant lectins that recognize specific glycan epitopes. To evaluate whether correlation analyses of lectin staining and glycan-related gene expression might provide useful information, we first performed lectin staining of a set of human B cells (Daudi, KMS-12BM, KMS-12PE, Namalwa, Raji, and Ramos) to obtain their cross-sample profiles of lectin epitope expression. We analyzed the strength of the correlations using Pearson's correlation coefficient, which is a standard, well-established method for assessing correlation. To prevent possible bias in the lectin choice, we used 15 plant lectins supplied in two commercially available sets.

To evaluate the efficacy of the calculations, the lectins were first divided into two groups based on the presence or absence of previous reports asserting a correlation between cell surface expression of a specific lectin epitope and expression of a certain glycosyltransferase gene. The lectins that lacked a reported correlation were divided into highly specific (or narrow) and broadly specific groups. The highly specific (narrow) lectins were further assigned to one of two subgroups according to the position of the epitope (terminal or interior) on the glycan chain.

CIRES correlation analyses of lectin staining profiles obtained using lectins with epitopes regulated by known biosynthetic enzyme genes

***Phaseolus vulgaris* leukoaggulutinin (PHA-L4)** PHA-L4 recognizes tri- or tetraantennary N-glycans with β_{1-6} branching of N-acetylglucosamine (GlcNAc), which often correlates with tumor progression [12]. Histochemical and immunoblot analyses have shown that PHA-L4 epitope expression correlates with the expression of the *MGAT5* (*GnT-V*) gene [13], and this lectin is commonly used as a marker for β_{1-6}-branched N-glycans. PHA-L4 epitope expression is diminished in *Mgat5*-null mice [14], and these mice exhibit enhanced rates of cytokine receptor internalization and subsequent cytokine signaling [15]. *MGAT5* expression was strongly correlated with the PHA-L4 staining profile, as shown in Figure 2A. The possible values of Pearson's correlation coefficient range between 1 and −1, where a value of 1 indicates complete correlation; therefore, the coefficient index between PHA-L4 staining and *MGAT5* expression (CI = 0.93) represents a highly significant correlation. Other correlated glycan-related genes were judged to be irrelevant to the biosynthesis of this epitope and are listed in Table S2, which contains the complete list of microarray-wide correlations for glycan-biosynthesizing genes.

The CIRES analysis correctly predicted that the *MGAT5* gene was responsible for expression of the PHA-L4 epitope. This prediction was confirmed by retrovirus-mediated gene expression in Namalwa B cells (Figure 2B). When a modified murine stem cell virus (MSCV) vector carrying genes for MGAT5 and enhanced green fluorescent protein (EGFP) divided with internal ribosomal entry site (IRES) *(MGAT5-IRES-EGFP)* was introduced into Namalwa cells, the level of PHA-L4 epitope expression was higher in the EGFP-positive population than in the EGFP-negative population. To rule out the possibility that viral infection somehow altered the cell surface glycan independently of glycosyltransferase expression, the vector carrying only *IRES-EGFP* was used as a negative control. In Namalwa cells expressing only EGFP, the EGFP-positive and EGFP-negative populations expressed identical levels of the PHA-L4 determinant (Figure 2B).

***Sambucus sieboldiana* agglutinin (SSA)** SSA recognizes α_{2-6}-linked Sia bound to galactose (Gal) or N-acetylgalactosamine (GalNAc). We previously showed that SSA epitope expression is induced in CHO cells by stable transfection with the rat *ST6GAL1* gene [11]. The deletion of *St6gal1* in mice eliminated the expression of the *Sambucus nigra* agglutinin (SNA) epitope [16], which is also recognized by SSA. In the present study, the correlation index was assessed to determine whether *ST6GAL1* gene expression correlated with SSA epitope expression, as determined by flow cytometry, in six B-cell lines. Although SSA staining in the six B-cell lines varied in intensity (Figure 2C), the staining profiles correlated with the gene expression profiles for *ST6GAL1* and a few other GlcNAc-transferase genes, including two β_{1-6} GlcNAc transferases and B3GNT5, which is involved in the biosynthesis of N-acetyllactosamine (LacNAc) units on glycan chains. These findings indicate that the SSA epitope detected by flow cytometry might be located at the terminus of poly-LacNAc units, which are often found on the β_{1-6} branch, and might extend beyond the glycocalyx of the cell surface.

***Arachis hypogaea* agglutinin (PNA)** PNA recognizes the Gal-exposed core-1 structure (Galβ_{1-3}GalNAc-Thr/Ser), and the capping of this epitope by sialylation severely reduces the affinity

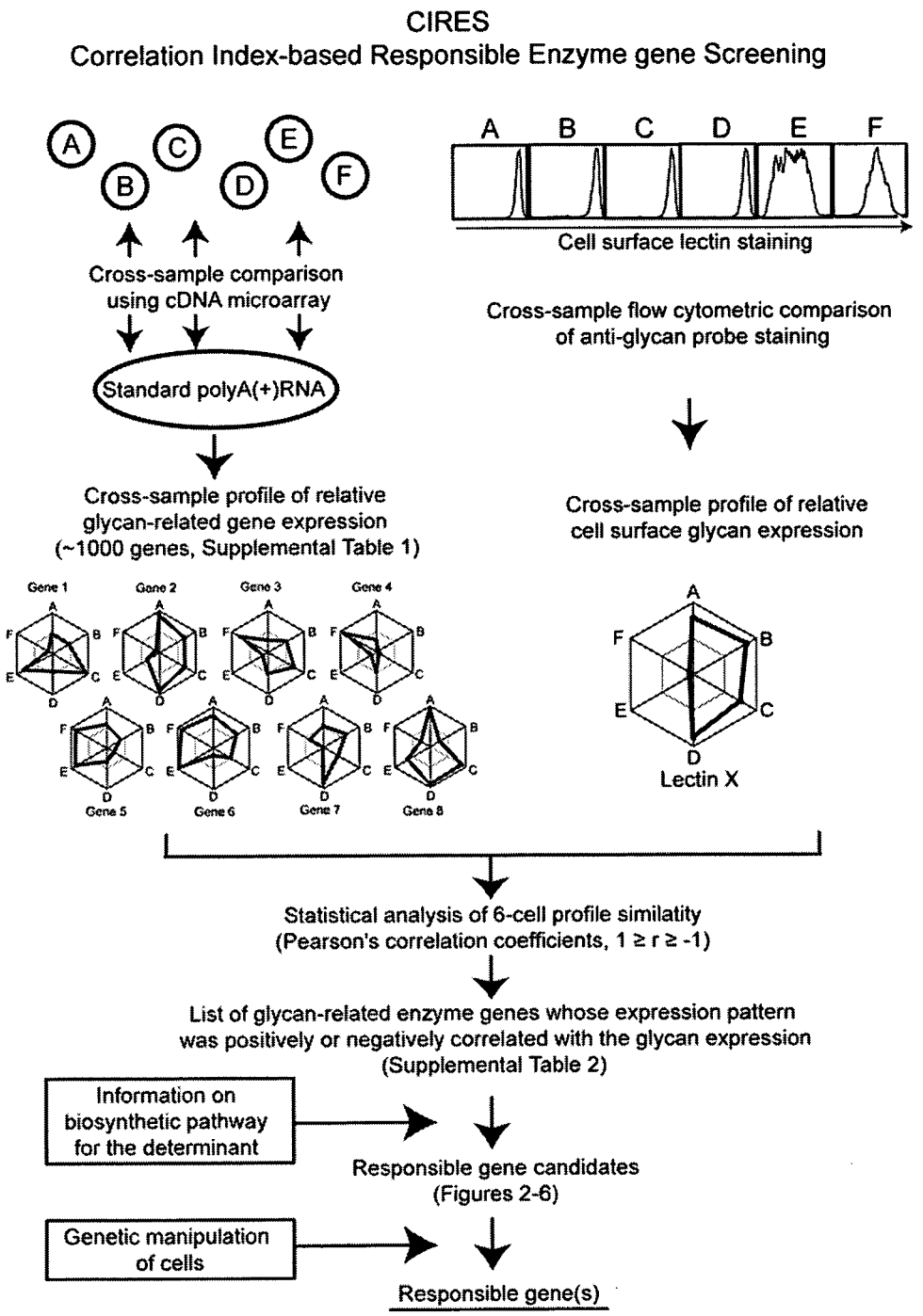

Figure 1. Schematic of the CIRES concept. The expression patterns of about 1000 glycan-related genes were profiled in a set of six different cell lines (A–F) by comparing the microarray binding of cellular cDNA and reference polyA(+) RNA and calculating the relative expression values (Table S1). The polygons in the left web graphs represent the relative gene expression profiles of eight glycan-related genes selected as examples. In these graphs, the difference in relative gene expression is expressed on a log scale, where the edge of the polygon corresponds to the strongest expression in each cell line (A–F). The same set of six cell lines were examined for cell-surface glycan expression using fluorescently labeled plant lectins and flow cytometry; the strength of the glycan expression is plotted as relative values among the six lines, where the edge of the polygon represents the strongest expression (web graph on top right). The glycan expression profiles were analyzed for correlations with the glycan-related gene expression profiles. Similarities and dissimilarities between the profiles were assessed using Pearson's correlation coefficient, which has values ranging from -1 (no correlation) to 1 (perfect correlation). A complete list of the genes found to be positively or negatively correlated with plant lectin staining patterns is presented in Table S2. Genes known to affect the biosynthesis of an epitope were selected from among the correlated genes (shown for each lectin in the tables on the right in Figures 2–6). A correlated gene identified by CIRES was confirmed as the gene responsible for regulating the biosynthesis of a particular glycan by transferring the gene into another cell line of the set, via gene transfer techniques such as retrovirus-mediated overexpression, and looking for a related change in epitope expression.
doi:10.1371/journal.pone.0001232.g001

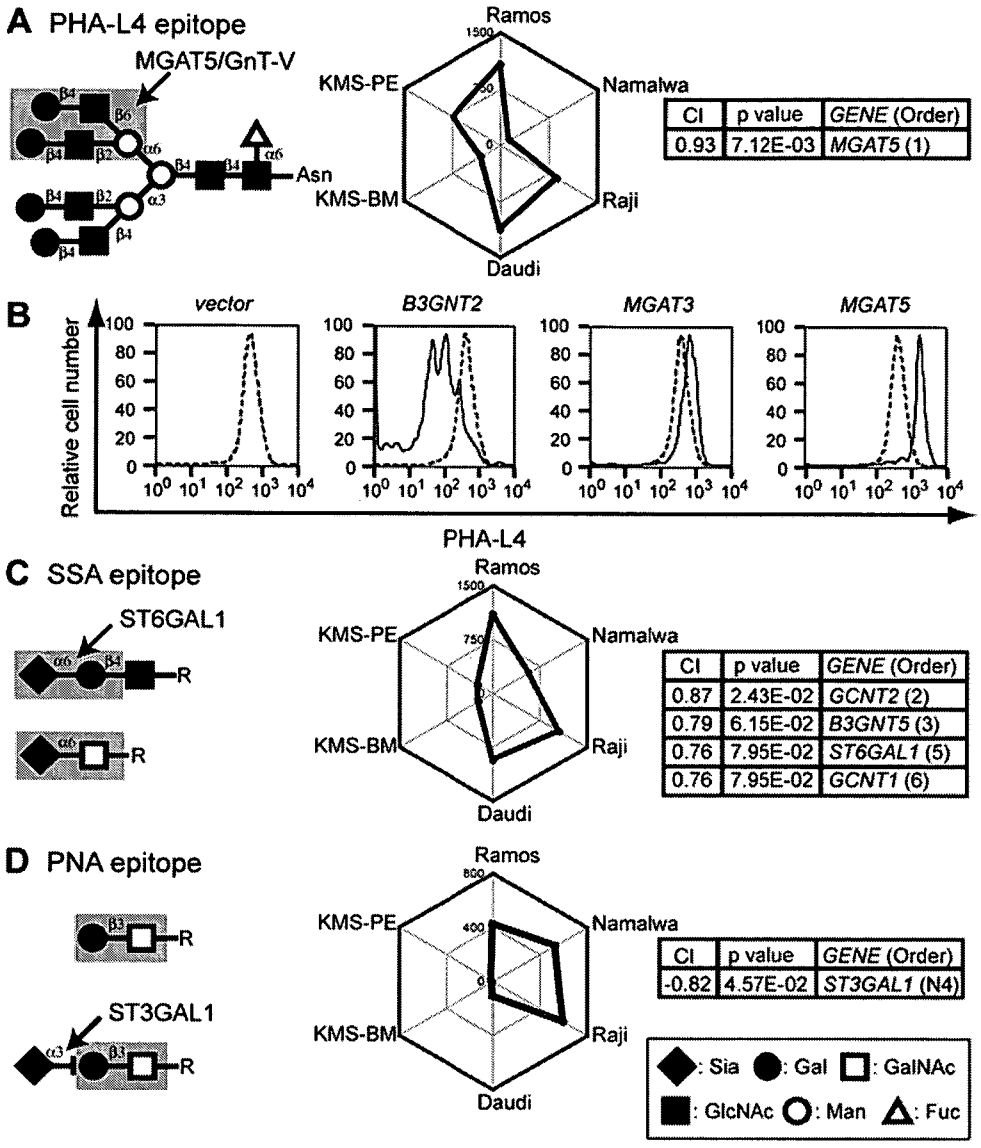

Figure 2. CIRES analyses of staining profiles obtained using lectins with known epitope expression-regulating enzymes. (A, C, D) Expected glycan structures for lectin recognition (left), web graphs of the lectin staining profiles (depicted as polygons) obtained using a set of six B-cell lines (middle), and the correlation indexes (CI, Pearson's correlation coefficient for profile matching) of the relevant genes that correlated with the plant lectin staining profiles and the *P* values of the correlations (right). The correlation orders of the glycan-related genes selected from the complete list of correlated genes (Table S2) are indicated as numbers in parentheses in the box for each gene, with a smaller number indicating a stronger correlation between gene expression and glycan expression profiles. Genes with a negative correlation are indicated by an N before the order number. The lectins used were **(A)** PHA-L4, **(C)** SSA, and **(D)** PNA. Lectin epitopes shown in the figures are taken from the literature unless otherwise specified [17,51]. **(B)** Namalwa cells were infected with MSCV harboring *MGAT5-IRES-EGFP*. Control cells were infected with empty vector (*IRES-EGFP*) or the same vector encoding *B3GNT2* or *MGAT3*. Flow cytometry results for PHA-L4 staining were compared between EGFP-positive cells (solid line) and EGFP-negative cells (dashed line).
doi:10.1371/journal.pone.0001232.g002

of the interaction [17]. Diminished PNA epitope expression reportedly coincides with an increase in α_{2-3} sialyltransferase activity, which sialylates the Gal residue [18]. This change was shown to occur during thymocyte maturation, in which PNA-positive cortex cells mature into PNA-negative medulla thymocytes. In a mouse model, the deletion of *St3gal1* caused a deficiency in the derepression of PNA reactivity during thymocyte development and eventually resulted in deficient $CD8^+$ T cell maturation [19].

The above findings suggest that the expression pattern of the PNA epitope might be positively affected by core-1 glycan biosynthesis and negatively affected by capping. Indeed, we found a negative correlation between PNA epitope expression and the *ST3GAL1* expression profile (Figure 2D). Thus, our correlation index analysis is able to not only identify a positive correlation but also reliably predict a negative correlation for a gene involved in the expression of a lectin glycan epitope.

Taken together, these results suggest that correlation indexing can be used to identify genes responsible for regulating cell surface expression of glycan epitopes, as determined by flow cytometry based on lectin binding. We designated this methodology as correlation index-based responsible-enzyme gene screening, or CIRES. After confirming that CIRES could be used to predict the genes involved in the biosynthesis of the glycan epitopes for these lectins (Figure 2), we used CIRES to assess the genes responsible

for the staining profiles of other plant lectins, as determined by flow cytometry.

CIRES correlation analyses of lectin staining profiles obtained using lectins that recognize specific terminal glycan structures and have unknown epitope expression-regulating enzyme genes

***Lens culinaris* agglutinin (LCA)** We assessed the staining profiles of lectins that recognize terminal structures of glycan chains. LCA recognizes the biantennary N-glycan chain with core α_{1-6} linked fucose (Fuc) attached to the chitobiose [20]. The presence of a core Fuc in the N-glycan of the Fc region of IgG severely represses the antibody-dependent cellular cytotoxicity activity of the antibody [21]. The expression of *FUT8* has been shown to be responsible for the biosynthesis of a core Fuc on N-glycans [22], but a correlation between *FUT8* gene expression and cell surface LCA staining has not been demonstrated in flow cytometry experiments.

Our analysis of the LCA staining profile and *FUT8* expression profile revealed a correlation (Figure 3A), although it was weaker than those for the three lectins described above (Figure 2). We also noted that *MGAT4b* gene expression negatively correlated with the LCA staining profile (Table S2). Considering that the presence of additional antennae on the N-glycan inhibits LCA binding [17], this type of negative correlation could be quite informative; however, in this case, no evidence was reported indicating that *MGAT4b* expression reduces the detection of the LCA epitope by flow cytometry. Nevertheless, CIRES is useful in predicting the genes involved positively or negatively in the biosynthesis of glycan epitopes.

***Ulex europaeus* agglutinin-I (UEA-I)** UEA-I recognizes α_{1-2}-linked Fuc on type-2 LacNAc, which is involved in forming the epitope of H-type human red blood cell antigen [23]. UEA-I staining did not reveal a significant positive correlation with the expression of the gene for α_{1-2} fucosyltransferase, which is involved in the biosynthesis of this linkage (Figure 3B). Instead, a prominent negative correlation was found with the expression profile of *ST3GAL6*, which has a preference for type-2 LacNAc substrates on both glycoproteins and glycolipids [24].

In theory, UEA-I binding should be affected by the expression of *FUT1* or *FUT2*, as they encode the proteins responsible for H antigen biosynthesis, and by the expression of A or B transferase, which can cap the H antigen to reduce the affinity [25]. However, the sequence similarity between the A and B (and also O) transferase genes prevented their differentiation in the microarray experiments. Redundant regulation by *FUT1* and *FUT2* in these cells may be the reason that no positive correlation with UEA-I epitope expression was observed. Alternatively, these data may suggest that negatively correlated ST3GAL6, which utilizes the same substrate as fucosyltransferases, may compete with the biosynthesis of this epitope by prior sialylation of the fucosyltransferase substrate(s).

***Ricinus communis* agglutinin (RCA120)** RCA120 preferentially recognizes terminal LacNAc structures found in various classes of glycans. These LacNAc structures are

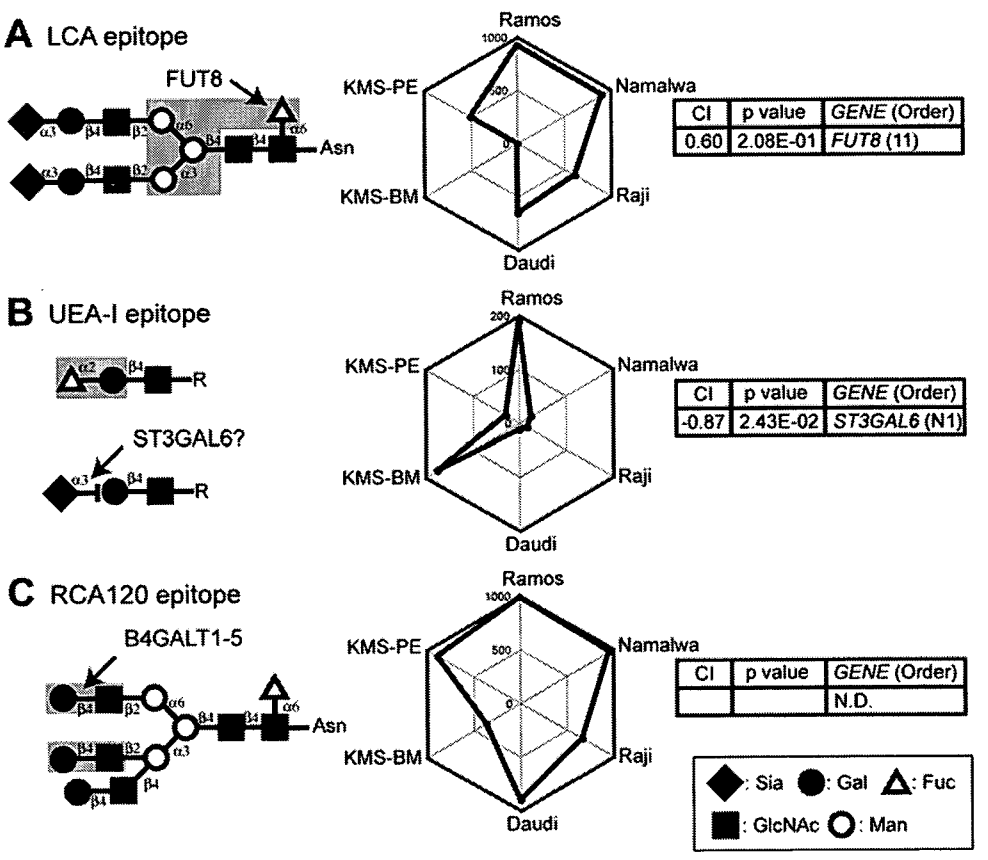

Figure 3. CIRES analyses of staining profiles obtained using lectins that recognize terminal glycan structures and have unknown epitope-expression-regulating enzymes. Presentation is the same as in Fig. 2 except that the plant lectins used were (A) LCA, (B) UEA-I, and (C) RCA 120. N.D. in the gene order list indicates that no gene was determined to have a correlation with the lectin staining.
doi:10.1371/journal.pone.0001232.g003

biosynthesized by a large group of B4GalT [26] and proximal GlcNAc-transferase family enzymes. The RCA120 staining profile revealed no obvious correlation with the genes for the enzymes known to be involved in this biosynthetic pathway (Figure 3C). Given our earlier correlation results identifying a terminal glycosyltransferase as being responsible for LacNAc expression (*i.e.*, sialyltransferase for SSA), this result was not surprising. It indicates that the abundant expression of LacNAc structures ensures the detection of a correlation between a terminal enzyme expression profile and the expression of a terminal glycan detected by flow cytometry. Moreover, capping of LacNAc should have a negative effect on its recognition by RCA120, which would make the detection of epitope expression more complex. It was clear that this procedure is not universally effective for lectin epitopes but that the effectiveness of the procedure depends on the type of glycan recognized by a lectin.

CIRES correlation analyses of lectin staining profiles obtained using lectins that recognize specific internal glycan structures and have unknown epitope expression-regulating enzyme genes

***Datura stramonium* agglutinin (DSA)** DSA recognizes tri- and tetraantennary N-glycans. It is specific for GlcNAc β_{1-4}-Man α_{1-3}-branched triantennary N-glycan [27,28], which is biosynthesized by MGAT4a and MGAT4b. In our experiments, the DSA staining profile resembled that of PHA-L4, and thus the two lectins correlated with similar genes, most prominently *MGAT5* (Figure 4A). This result could be explained by the fact that the addition of a β_{1-6} branch increases the preference of DSA for a ligand, even though MGAT4a/b activity is required. Ihara et al. have reported that DSA staining correlates with the expression level of *MGAT5* in *in vitro*-differentiated GOTO cells [29], suggesting that *MGAT5* may also be involved in the biosynthesis of the optimal DSA epitope, with a tetraanntenary glycan. Consistent with this idea, the introduction of *MGAT5* into Namalwa cells resulted in a 60% increase in DSA staining (Mean fluorescence intensity (MFI), 1986), compared with control (MFI, 1247) (Figure 4B). Interestingly, when *MGAT3* was introduced into Namalwa cells, DSA epitope expression was subtly suppressed (MFI, 961) compared with control expression (MFI, 1222), possibly due to the competitive relationship between MGAT3 and MGAT5 [30] (Figure 4B). These effects appeared to be specific, because no obvious shift was seen in cells with introduced *B3GNT2*.

***Phaseolus vulgaris* erythroagglutinin (PHA-E4)** The staining profile of PHA-E4 was similar to those of PHA-L4 and DSA. This result was unexpected because PHA-E4 recognizes bisecting GlcNAc-containing biantennary N-glycans, which comprise a type of glycan distinct from the PHA-L4 epitope. Owing to the similarity among the staining patterns of these three lectins, a correlation was also found between PHA-E4 staining and *MGAT5* (Table S2), but PHA-E4 staining did not correlate with *MGAT3* (*GnT-III*), which is the GlcNAc transferase gene expected to correlate by virtue of its known epitope specificity (Figure 4C). However, when we overexpressed *MGAT3* in Namalwa cells, the MFI value of PHA-E4 staining increased, from 873 in the control population to 1868 in the EGFP-positive population (Figure 4D). Thus, the expression level of *MGAT3* appears to be important for PHA-E4 epitope biosynthesis, as expected. The overexpression of *MGAT5* had no effect on PHA-E4 binding; the MFI value was 899 in the control population and 866 in the EGFP-positive population.

When we stained the membrane fractions from the six B-cell lines using PHA-E4 in lectin-blot analyses, the blot and FACS signal strengths differed, as seen in the shape of the staining profile (Figure 4E), and *MGAT3* expression did not correlate with the signal strength on the lectin blot. Somewhat consistent with our result, Miyoshi et al. reported that *MGAT3* expression levels did not necessarily correlate with cell-surface staining of the PHA-E4 ligand in flow cytometry experiments, although co-expression was found in lectin-blot experiments [31]. Thus, our results support the suggestion of Miyoshi et al. that the cell-surface expression level of the PHA-E4 ligand epitope may be regulated by factor(s) other than *MGAT3* expression. Consistent with this idea, they also reported that the presence of bisecting GlcNAc negatively affected the sorting of glycoproteins to the cell surface [32].

CIRES correlation analyses of lectin staining profiles obtained using lectins that recognize multiple glycan structures

Some of the lectins used in the present study had mixed or heterologous specificity. We assessed the correlation indexes for the staining profiles of these lectins.

***Maackia amurensis* lectin (MAM)** MAM is a mixture of two lectin subunits, MAL and MAH. MAL binds to Sia α_{2-3}-LacNAc structures [33], whereas MAH preferentially recognizes disialylated structures found in O-glycans [34]. Of the known sialyltransferases, ST3GAL3, ST3GAL4, or ST3GAL6 may synthesize the MAL epitope, and ST8s may synthesize disialylated glycans. Correlation-index analyses showed that *ST3GAL3* and *B3GNT2* may be responsible for the expression of the epitope in the six B-cell lines (Figure 5A). This is consistent with a previous report that repeating LacNAc units enhance MAL binding [35]. The MAL binding preference seemed to be more important than that of MAH in this CIRES prediction based on MAM staining and flow cytometry. As expected from its positive correlation with *B3GNT2* expression, the MAM epitope showed increased levels in Namalwa cells overexpressing *B3GNT2*, whereas overexpressed *MGAT3* was negatively correlated with the MAM staining profile, owing to the suppression of MAM epitope expression (Figure 5B). Thus, the MAM epitope may be preferentially biosynthesized on LacNAc units of the β_{1-6} branch of N-glycans. Alternatively, MGAT3 expression may change the sorting of the protein carrying the MAM epitope. Taken together, these results indicate that the expression of correlated genes can have an additive regulatory effect (positive or negative) on the cell-surface presentation of a lectin epitope.

***Triticum vulgaris* agglutinin, wheat germ agglutinin (WGA)** WGA is thought to preferentially recognize clustered N-acetyl groups found in N-acetylneuraminic acid (Neu5Ac), GlcNAc, and GalNAc. Neu5Ac is often a major WGA ligand because the Sia density on the termini of glycan chains tends to increase for the highly branched N-linked glycans [17]. The affinity of WGA for Sia was exploited in the isolation of Lec mutants in CHO cells [36]. The density of the N-acetyl group can also be high in the I-branched β_{1-6} GlcNAc-containing glycans [17].

The WGA staining profile correlated strongly with the expression profile of the *ST6GAL1* gene and weakly with that of the *ST3GAL3* gene (Figure 5C). (These genes were previously known as *ST6N* and *ST3N*, respectively [37].) Since WGA binding to sialylated glycans increases with the degree of sialylation, this correlation pattern seems to indicate that the supply of the substrate LacNAc is ample and that expression of the terminal sialyltransferases determines the expression level of the WGA epitope. Among these sialyltransferases, *ST6GAL1* appeared to play a more prominent role in biosynthesis in the B-cell lines used in this study. In addition to the I-branching β_{1-6} GlcNAc transferase [38], *GCNT2* expression also correlated with WGA

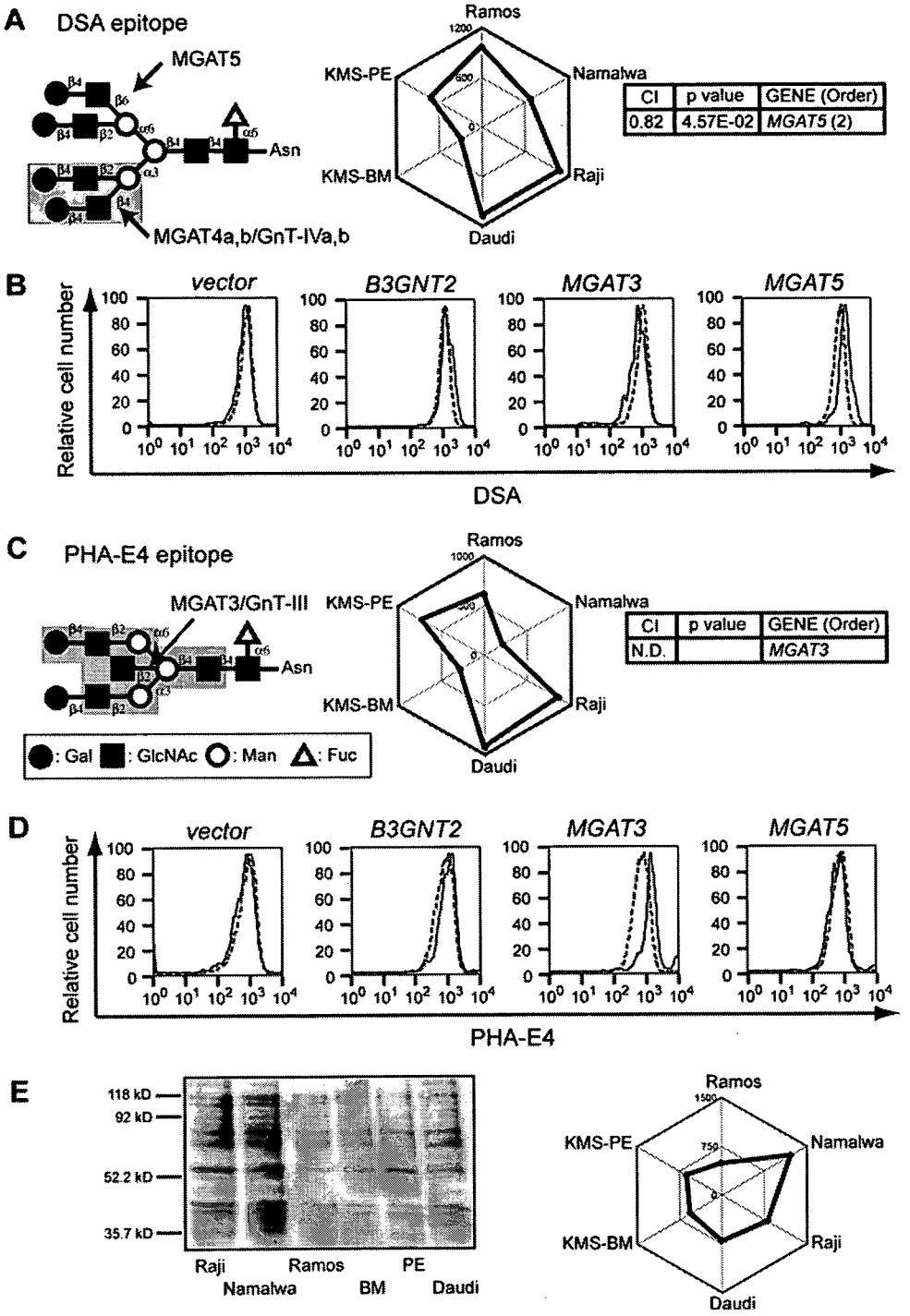

Figure 4. CIRES analyses of staining profiles obtained using lectins that recognize internal glycan structures and have unknown epitope-expression-regulating enzymes. Presentation is the same as in Fig. 2 except that the plant lectins used were **(A, B)** DSA and **(C–E)** PHA-E4. N.D. in the gene order list indicates that no significant correlation was detected. **(B, D)** Flow cytometric staining patterns for EGFP-positive Namalwa cells are shown in bold lines, and those for EGFP-negative (control) cells are shown in gray dashed lines. The overexpression of *MGAT5* resulted in a subtle (60%) increase in DSA staining. The overexpression of *MGAT3* resulted in a 2-fold increase in PHA-E4 staining. **(E)** PHA-E4 lectin blotting was performed using the membrane fraction of the same set of cell lines. A plot of the quantified signals reveals differences in the PHA-E4 staining profile among the six cell lines (C, E), as discussed in the text.
doi:10.1371/journal.pone.0001232.g004

staining, probably reflecting the GlcNAc-binding aspect of WGA. In a case such as this one, the correlation of the genes identified by CIRES may appear to be additive, but a lack of exclusivity tends to reduce the correlation index for each gene.

***Canavalia ensiformis* lectin (Con-A)** The modification of N-glycans occurs following the transfer of lipid-linked Glc_3-Man_9-$GlcNAc_2$ to nascent N-glycosylated protein by oligosaccharyl-transferase in the ER [39]. Con-A recognizes mannose (Man)-

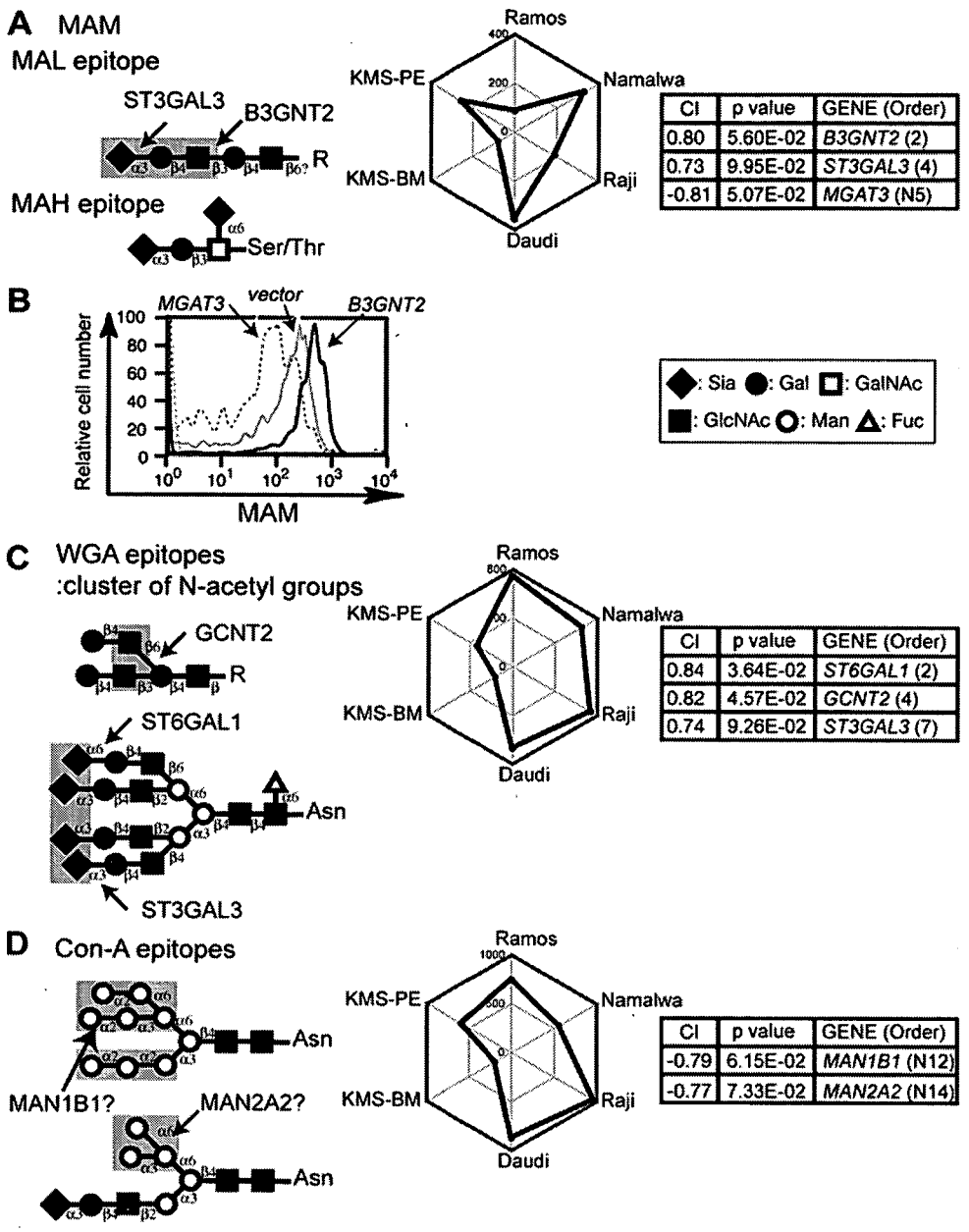

Figure 5. CIRES analyses of staining profiles obtained using lectins that recognize multiple glycan structures and have unknown epitope expression-regulating enzymes. Presentation is the same as in Fig. 2 except that the plant lectins used were (A–B) MAM, (C) WGA, and (D) Con-A. The epitopes of the two different lectins of MAM, MAL and MAH, are illustrated separately. WGA essentially recognizes a cluster of N-acetyl groups, as indicated, and thus required Neu5Ac as a Sia species. Con-A recognizes mannose-containing glycans with varying affinities. High-mannose-type glycans (upper diagram in (D)) bind best to this lectin. (B) Namalwa cells were infected with retroviruses encoding various GlcNAc transferases. The MAM staining patterns of the EGFP-positive populations of each infectant are shown. *MGAT5* overexpression did not shift the staining pattern in comparison with the vector control (data not shown).
doi:10.1371/journal.pone.0001232.g005

containing N-glycans to various degrees; it binds preferentially to high-mannose N-glycans, followed by hybrid-type N-glycans, and has the least affinity for complex-type N-glycans. In theory, oligosaccharyltransferase activity is required for the expression of the Con-A epitope, whereas mannosidase expression is inhibitory. Con-A staining profiles revealed a subtle but significant negative correlation with the expression of the mannosidase genes *MAN1B1* and *MAN2A2* (Figure 5D). Thus, the mannosidases encoded by these genes may control the expression of high-mannose N-glycans on the cell surface. Alternatively, other factors such as the expression of the protein moiety of the glycoconjugate could determine the expression of the Con-A epitope, given that the number of proteins reported to carry high-mannose glycans is limited.

***Agaricus bisporus* agglutinin (ABA)** ABA recognizes Gal-exposed core-1 structures that are similar to the PNA epitope, but in contrast to PNA, ABA can recognize sialylated structures [40]. In B cells, ABA staining was similar to PNA staining and was negatively correlated with *ST3GAL1* expression (Figure 6A). Consistent with this negative correlation, ABA binding was increased in Daudi cells treated with sialidase (Figure 6B), similar to the enhanced binding of PNA observed upon sialidase treatment. This effect occurred with both a broad-range sialidase

(*Arthrobacter ureafaciens* sialidase, AUS) and the $\alpha_{2,3}$-linked Sia-specific *Salmonella typhimurium* sialidase (Figure 6B), indicating that sialylation, which probably occurs on the core-1 Gal residue, somehow inhibits recognition by ABA.

B3GNT5 expression positively correlated with ABA staining. In fact, a recent study has shown that ABA has dual specificity for glycan chains, recognizing both Gal-exposed O-glycans and GlcNAc-exposed N-glycans [41]. Whether the GlcNAc residue biosynthesized by the GlcNAc transferase is uncapped on the cell surface is unknown, but some ABA binding to GlcNAc may contribute to the increased correlation index of *B3GNT5* as compared with that for PNA, which showed an otherwise similar staining profile for the correlated genes.

Overall findings

As confirmed by staining with various plant lectins, CIRES successfully identified enzyme genes known to be involved in the biosynthesis of lectin-binding determinants. When an unbiased set of 15 lectins was analyzed for binding to six B-cell lines, 12 of the lectins showed significant staining. Correlation assessment of these staining profiles identified the enzyme genes that are apparently responsible for the expression of the specific epitopes for nine lectins. In general, lectins that recognize terminal structures of the glycan chain tended to yield the most reliable correlation with the responsible genes.

Interestingly, CIRES also found negative correlations for some epitopes, which is consistent with the fact that CIRES results are highly dependent on the regulatory mechanisms of glycan epitope expression, some of which are negative (*i.e.*, capping of an epitope by further glycosylation). Finding negative relationships is difficult in normal biological experimental setups but may have been possible using CIRES because of the unbiased correlation coefficient calculation resulting from the large set of cross-sample comparisons.

DISCUSSION

CIRES correlation analysis of glycan-related gene expression and binding of anti-glycan probes such as lectins

The functional glycans expressed on a cell surface can encode biological information. Although glycan-glycan interactions are important in determining the biological consequences of some glycosylations [42], glycan-binding proteins are the major target of functional glycans. Thus, the binding of glycan-specific proteins can be highly informative in decoding the glycomic information of an organism [43], making glycan-binding proteins a rational choice for the analysis of glycan expression. Although the identification of the proteins that bind best to each glycan is no doubt important given the role of glycan-binding proteins in glycan recognition in an organism [44,45], here we opted to

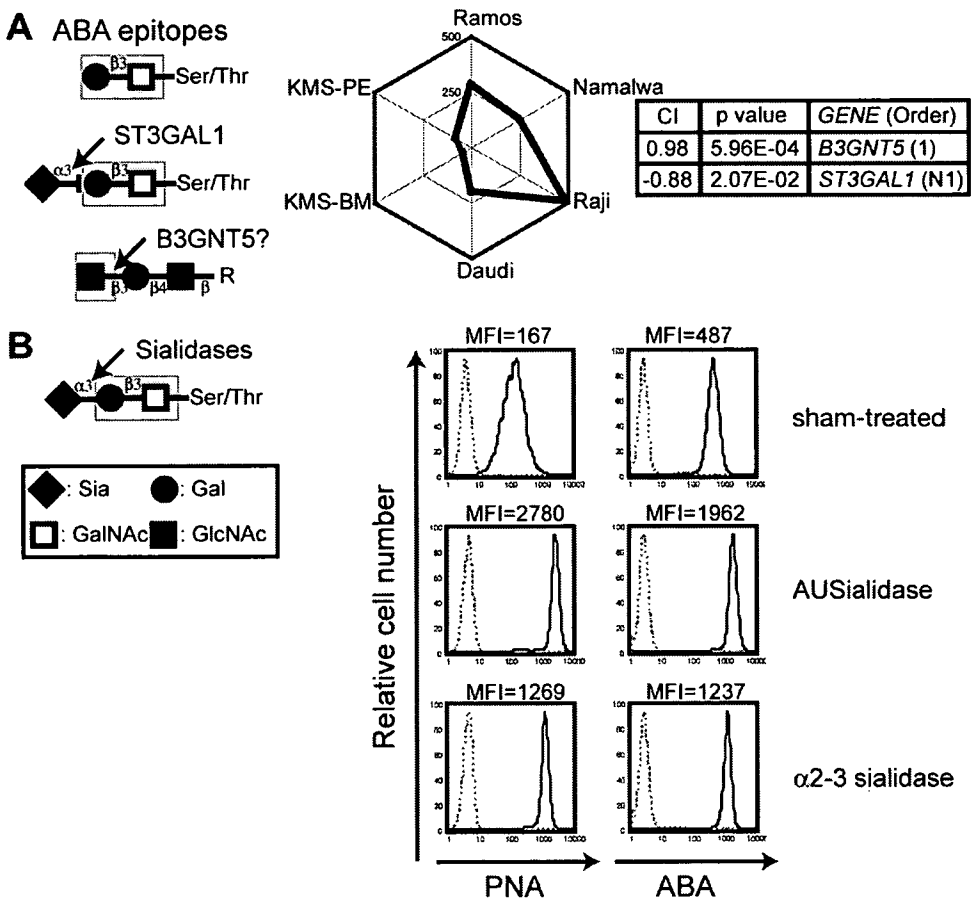

Figure 6. CIRES analyses of staining profiles obtained using the lectin ABA. (A) Presentation is the same as in Fig. 2 except that ABA was used. **(B)** Effect of sialidase treatment on the binding of ABA and PNA in B cells. (See text for the specificity of the sialidase and Fig. 2D for the PNA epitope.) Mean fluorescence intensity (MFI) values for the staining with each lectin (bold lines) are shown at the top. Dashed lines indicate the results from the non-staining control.
doi:10.1371/journal.pone.0001232.g006

identify the genes involved in the biosynthesis of specific glycans because, as the glycan-biosynthesis enzymes are responsible for producing the glycan ligands, this information will help elucidate the regulation of biological events mediated by glycan-binding proteins.

Systematic methodological merit of CIRES

The experimental setup for CIRES is relatively simple. Briefly, we first made a cross-sample comparison of glycan-related gene expression profiles using cDNA microarrays. This technique yielded the relative expression level for each gene as compared with a universal reference RNA, producing an expression profile for each gene. We then used anti-glycan lectin probes to obtain binding profiles in the same cell lines and compared the two types of profiles. We used the same cross-sample profiles of glycan-related gene expression for the correlation analyses of all the lectins examined in this study.

The cells that we used for gene expression profiling are available either commercially or from a non-profit cell resource center (Japanese Collection of Research Bioresources; JCRB). All cells were cultured under commonly used conditions and were used in logarithmic growth phase. Under these conditions, the glycan expression phenotype obtained by lectin staining tended to be uniform within a cell line and unique for each cell line. Thus, the data obtained by lectin staining with excess probe were suitable for determining the mean fluorescence intensity (MFI) of lectin staining.

This method compared the relative glycan expression profiles of cell lines whose cellular size and character might not be uniform; therefore, we normalized the staining signal by using the ratio of the stained sample MFI to the control MFI. This eliminates the absolute glycan expression signals and normalizes the relative expression results to the staining and data acquisition conditions.

The statistical analysis is the core of the CIRES method. Since glycosylation follows a defined pathway, we could have set up an algorithm suitable for the correlation analyses. However, we chose to use the well-established Pearson's correlation coefficient for the analyses. Regardless of the calculation method, correlations were detected even when the profiles did not completely match. Based on these calculations, a list of genes can be ordered according to the strength of their correlation. This list might be useful in designing further experiments to confirm biological functions.

In glycan biosynthesis, not all relationships are positive in nature, and some lectins used in this study yielded negative correlations. Thus, it is possible to detect dominant inhibitors of specific glycan biosynthesis steps using CIRES. Moreover, in theory, CIRES is not limited to glycan biosynthesis but could be used in any system for which numeric phenotypic expression results (such as glycan expression) can be obtained for a set of cultured cells. The correlation of non-glycosylation phenotypes with gene expression in the same system should be possible.

Systematic methodology for using microarray data in CIRES

One limitation of the standard microarray technique is that it can only detect the relative cDNA expression levels of two samples. This was actually useful when we took the ratio of the signal for each gene relative to that for reference RNA, thus circumventing the microarray problems associated with spot-to-spot variation and hybridization variation for different nucleotide sequences. Almost all of the spots hybridized with universal reference RNA (data not shown). Normal, uniform cell culture conditions were used in this experiment to maximize reproducibility.

In order to calculate the gene expression ratios in a cross-sample manner, we wanted to avoid negative signals in the microarray scans. To do this, we directly used the raw data, instead of applying a cut-off value to the microarray signal by deducting the local background signal from the raw spot signals. We consider this to be a valid option, because we confirmed that the scanner readout after hybridization was reproducible, even for spots yielding weaker signals, and that both options yielded a similar order of relative strength (data not shown).

Normalization was also important because the array results were compared in a cross-sample manner. Sum-based normalization was applied to obtain better correlation coefficients for proven lectins (data not shown). The validity of the calculations was dependent on the use of a consistent standard, making a universal reference essential for the cross-sample comparison. In general, the microarray results tended to be more consistent for stronger hybridization signals than for weaker signals.

Expected and unexpected findings with CIRES

For an epitope whose expression is regulated by a single gene product in its biosynthetic pathway and for which the supply of substrate for that biosynthetic reaction is abundant, CIRES will identify the gene involved in the biosynthesis of the epitope. The finding that the RCA120staining profile did not correlate with a specific glycosyltransferase was therefore not surprising, because it binds LacNAc. Generally, we obtained better correlation coefficients for epitopes created by terminal modifications of LacNAc. CIRES was also useful in identifying major genes responsible for epitope capping, which is negatively correlated with glycan expression, as in the case of PNA.

Our CIRES results tended to show correlations with the GlcNAc transferases. This may result from the use of flow cytometry to detect lectin binding, and thus glycan expression, because lectin staining preferentially detects glycans that extend beyond the glycocalyx. Moreover, the level of epitope expression may not linearly correlate with the lectin signal, because lectins tend to form multimers. As poly-LacNAcs are the usual core units for the presentation of some functional glycan epitopes, GlcNAc transferases found to correlate could also be important for the epitope presentation suitable for lectin-based recognition.

Thus far, we have not identified any enzymes other than glycosyltransferases that strongly correlate with epitope expression levels. However, a subtle negative correlation was noted between the expression of the Con-A epitope and mannosidase expression. Our failure to identify additional enzymes might have resulted from the limited number of lectins available to us. In theory, other factors involved in biosynthetic pathways, such as factors involved in sugar-nucleotide biosynthesis or transport, could also regulate glycan expression on the cell surface.

Limitations of CIRES

Specific probes are unquestionably important for the successful application of CIRES. The most important aspect of lectin specificity is not affinity for the glycan ligand but rather the exclusivity of the enzyme. To calculate statistically significant correlations, a set of cell lines expressing different amounts of the target glycan should be used. The uniform expression of the target glycan in the cell set is undesirable.

To evaluate this methodology, we used the plant lectins that have been used extensively in other glycan studies. Since the correlations are identified by statistical calculations alone, we first assessed those lectins that had already been correlated with specific enzyme genes, to test for the identification of genes that matched glycan expression only by chance. Therefore, when CIRES is applied using uncharacterized glycan-binding probes, the bi-

ological relevance of the correlated genes must be confirmed by altering their expression in the cells. This requirement could be viewed as a limitation of the system. However, the alteration of target glycan expression has been an enduring and major objective of glycobiological experiments concerning lectins. As indicated in Figure 1, the CIRES methodology includes confirmation of the correlation by using glycan-related gene overexpression or silencing. Confirming biological relevance via the transfer of a correlated gene has the additional benefit of providing cells with a different expression level of the epitope of interest, which can be valuable for further assessment of lectin recognition in biological systems. Changing the cell surface expression of glycans for specific anti-glycan probes has been difficult, because the rate-limiting glycosyltransferase must be identified and overexpressed. Thus, allowing for a glycan-related gene transfer procedure that produces glycan-altered cells for further experiments is a major merit of the CIRES methodology.

CIRES alone cannot identify the specific glycan structure to which an anti-glycan probe binds; at the same time, knowledge of the structure of interest does not necessarily mean that modifying its expression on cells is possible. Using the CIRES method will likely result in the production of cells with modified glycan expression, but the actual structure bound by the probe may be unknown. This situation is somewhat similar to that of glycan-array binding studies, in which the probe that binds best on the glycan array does not necessarily bind the same glycan on the array as on cells and the identification of the glycan structure does not always result in the identification of the relevant biosynthetic enzyme. Thus, CIRES could be combined with conventional glycan-binding assays [44–46] to determine the specificity of glycan binding in a set of glycans and to identify the gene that modulates glycan expression on the cell surface, from among the pathway component enzymes. Thus, CIRES is a highly useful genetic strategy for studying the functionality of the interactions between glycans and glycan-binding proteins in cell-based systems.

MATERIALS AND METHODS

Reagents and cell culture

Two commercially available sets of biotin-conjugated plant lectins (Plant Lectin Set I and II) were obtained from Seikagaku (Tokyo, Japan). R-Phycoerythrin-conjugated streptavidin was obtained from Caltag (USA). The B-cell lines Daudi, Namalwa, Raji, Ramos, KMS-BM, and KMS-PE were obtained from the Japanese Collection of Research Bioresources and were cultured in RPMI 1640 medium supplemented with 10% fetal bovine serum, sodium pyruvate, non-essential amino acids, and 2-mercaptoethanol.

DNA microarrays

Gene expression profiling of the six B-cell lines was performed using a glycan-focused cDNA microarray (RIKEN human glycogene microarray, version 1) and a GEO Platform (GPL #3465) and compared with reference RNA (Clontech, USA) to create GEO Series GSE 4407, as reported elsewhere [11].

Flow cytometry

A total of 2.5×10^5 B cells in 100 μl FACS buffer (1% BSA and NaN_3 in PBS(–)) was incubated with excess biotinylated plant lectin probes at room temperature for 30 min. R-Phycoerythrin- or FITC-conjugated streptavidin was used to detect lectin binding. Data were obtained using FACScan or FACSCaliber (BD Biosciences, USA) and analyzed using FlowJo (Tristar, USA) or Cellquest software (BD Biosciences, USA). To cross-compare staining signals between cell lines, the mean fluorescence intensity (MFI) of the background staining was adjusted to around 10, and the relative staining signal was expressed as the ratio of sample MFI divided by the control MFI.

Statistical analysis

Fluorochrome signals on the microarray were acquired by an array scanner (Affymetrix 428) without background subtraction and were then background-corrected using a smoothing function [47]. They were then Lowess normalized using Linear Models for Microarray Data (LIMMA) [48] and the software program R [49]. Inter-array normalization was not used in cross-sample comparisons, as it seemed to cause over-normalization.

The signal from the B-cell lines was divided by the signal from the universal reference RNA [11] to obtain the relative expression profile for each gene in each cell line (Table S1). The gene expression profiles were compared with the lectin staining profiles obtained by flow cytometry. Similarities between the profiles were evaluated with Pearson's correlation coefficient, and probability values (P) were calculated using the correlation coefficient test. For a sample size of six, a correlation coefficient of 0.81 indicates a statistical significance level of 5%. The genes that correlated with lectin staining by this method were ranked according to correlation strength (Table S2), and this list was examined for genes that appeared to be relevant to previously reported lectin glycan epitopes and glycan biosynthetic pathways (Figure 1).

Retrovirus-mediated transduction of glycan-related genes

Retroviruses were prepared and were used to infect Namalwa cells, as reported previously [11]. Briefly, full-length glycosyltransferase cDNA was cloned into a modified MSCV vector, which expressed cDNA and EGFP via an internal ribosome entry site. The plasmid was transiently transfected into Plat-A packaging cells [50], and retrovirus-containing supernatants were collected. Namalwa cells were spin-infected (2000 rpm, 32°C, 120 min) with the retrovirus in the presence of 6 μg/ml polybrene.

The retrovirus-infected cells were cultured for 2 days after infection before analysis by flow cytometry. EGFP-positive and -negative cells were regarded as infected and non-infected cells, respectively. The staining of these two populations was used as the control.

Lectin blotting

B cells were sonicated in detergent-free lysis buffer [10 mM Tris-HCl (pH 7.6), 1 mM DTT, 1 mM EDTA, 0.25 M sucrose, and protease inhibitor cocktail (Roche)]. Postnuclear supernatants were further ultracentrifuged, and the pellets (membrane fraction) were resuspended in lysis buffer. The suspensions were subjected to lectin blotting with HRP-conjugated PHA-E4. The signal intensity was measured by exposure of the membrane to LAS300 (Fujifilm, Japan).

Sialidase treatment

Sialidase treatment was carried out as reported elsewhere [11]. Briefly, Daudi cells were incubated with sialidase in 100 mM sodium acetate (pH 5.2) at room temperature prior to lectin staining. Sialidases from *Arthrobacter ureafaciens* (AUS; Calbiochem, San Diego, USA) and *Salmonella typhimurium* (Takara, Kusatsu, Japan) were used.

SUPPORTING INFORMATION

Table S1 Complete gene expression profiles obtained from cDNA microarray: Fluorescent Cy3 (universal reference) and Cy5

(each Bcell line) readout data were acquired from the array scanner and following statistical calculations were applied using the software program R. First, background was corrected using "Edward method". Each data was then normalized using Linear Models for Microarray Data (LIMMA) to correct bias between fluorescent dyes. Finally, the Cy5 signal from the B cell lines was divided by the Cy3 signal to obtain the relative expression profile for each spot and resultant relative values were shown in columns I through N for each cells. Column A shows serial number of all spots on microarray and column B through E show physical location of all spots on glass slide-based cDNA microarray.
Found at: doi:10.1371/journal.pone.0001232.s001 (0.31 MB XLS)

Table S2 Lists of correlated genes with lectin staining: This is an Exel file consists of 14 worksheets. First sheet shows full list of genes spotted on the Glycan-focuesed microarray and their gene ID numbers. Following sheets are the lists of genes that exhibited stronger correlation with indicated lectin staining profiles. See "Materials and Methods" for the method applied for calculation.
Found at: doi:10.1371/journal.pone.0001232.s002 (0.40 MB XLS)

ACKNOWLEDGMENTS

The authors thank Dr. Hisashi Narimatsu (AIST) for full-length cDNA clones of glycosyltransferases and Dr. Toshio Kitamura (University of Tokyo) for Plat-A packaging cells. We also thank Drs. Atsushi Kuno (AIST) and Eiji Miyoshi (Osaka University) for helpful discussions about lectin determinants.

Author Contributions

Conceived and designed the experiments: HT YK HY AS YO. Performed the experiments: YN RF HY. Analyzed the data: HT YN RF HY YO GT. Contributed reagents/materials/analysis tools: HT YK AS YO GT. Wrote the paper: HT.

REFERENCES

1. Freeze HH (1999) Monosaccharide Metabolism In: Varki A, Cummings R, Esko JD, Freeze HH, Hart GW, Marth J, eds. Essentials of Glycobiology. New York: Cold Spring Harbor Laboratory Press. pp 69–84.
2. Hirschberg CB, Robbins PW, Abeijon C (1998) Transporters of nucleotide sugars, ATP, and nucleotide sulfate in the endoplasmic reticulum and Golgi apparatus Annu Rev Biochem 67: 49–69 9759482.
3. Kornfeld R, Kornfeld S (1985) Assembly of Asparagine-Linked Oligosaccharides Annu Rev Biochem 54: 631–664.
4. Aruffo A, Seed B (1987) Molecular cloning of a CD28 cDNA by a high-efficiency COS cell expression system Proc Natl Acad Sci U S A 84: 8573–7 2825196.
5. Seed B, Aruffo A (1987) Molecular cloning of the CD2 antigen, the T-cell erythrocyte receptor, by a rapid immunoselection procedure Proc Natl Acad Sci U S A 84: 3365–9 2437578.
6. Larsen RD, Rajan VP, Ruff MM, Kukowska-Latallo J, Cummings RD, et al. (1989) Isolation of a cDNA encoding a murine UDPgalactose:beta-D-galactosyl-1,4-N-acetyl-D-glucosaminide alpha-1,3-galactosyltransferase: expression cloning by gene transfer Proc Natl Acad Sci U S A 86: 8227–31 2510162.
7. Narimatsu H (2004) Construction of a human glycogene library and comprehensive functional analysis Glycoconj J 21: 17–24 15467393.
8. Comelli EM, Head SR, Gilmartin T, Whisenant T, Haslam SM, et al. (2006) A focused microarray approach to functional glycomics: transcriptional regulation of the glycome Glycobiology 16: 117–31 16237199.
9. Takematsu H, Kozutsumi Y (2007) DNA microarray in glycobiology In: Greet-Jan B, Lee YC, Suzuki A, Taniguchi N, Voragen AGJ, eds. Comprehensive Glycoscience vol. 2. Oxford: Elsevier. pp 428–448.
10. Kawano S, Hashimoto K, Miyama T, Goto S, Kanehisa M (2005) Prediction of glycan structures from gene expression data based on glycosyltransferase reactions Bioinformatics 21: 3976–82 16159923.
11. Naito Y, Takematsu H, Koyama S, Miyake S, Yamamoto H, et al. (2007) Germinal center marker GL7 probes activation-dependent repression of N-glycolylneuraminic acid, a sialic acid species involved in the negative modulation of B cell activation Mol Cell Biol 27: 3008–3022.
12. Fernandes B, Sagman U, Auger M, Demetrio M, Dennis JW (1991) Beta 1-6 branched oligosaccharides as a marker of tumor progression in human breast and colon neoplasia Cancer Res 51: 718–23 1985789.
13. Yamamoto H, Swoger J, Greene S, Saito T, Hurh J, et al. (2000) Beta1,6-N-acetylglucosamine-bearing N-glycans in human gliomas: implications for a role in regulating invasivity Cancer Res 60: 134–42 10646865.
14. Granovsky M, Fata J, Pawling J, Muller WJ, Khokha R, et al. (2000) Suppression of tumor growth and metastasis in Mgat5-deficient mice Nat Med 6: 306–12 10700233.
15. Partridge EA, Le Roy C, Di Guglielmo GM, Pawling J, Cheung P, et al. (2004) Regulation of cytokine receptors by Golgi N-glycan processing and endocytosis Science 306: 120–4 15459394.
16. Hennet T, Chui D, Paulson JC, Marth JD (1998) Immune regulation by the ST6Gal sialyltransferase Proc Natl Acad Sci U S A 95: 4504–9 9539767.
17. Kuno A, Uchiyama N, Koseki-Kuno S, Ebe Y, Takashima S, et al. (2005) Evanescent-field fluorescence-assisted lectin microarray: a new strategy for glycan profiling Nat Methods 2: 851–6 16278656.
18. Gillespie W, Paulson JC, Kelm S, Pang M, Baum LG (1993) Regulation of alpha 2,3-sialyltransferase expression correlates with conversion of peanut agglutinin (PNA)+ to PNA- phenotype in developing thymocytes J Biol Chem 268: 3801–4 8440675.
19. Priatel JJ, Chui D, Hiraoka N, Simmons CJ, Richardson KB, et al. (2000) The ST3Gal-I sialyltransferase controls CD8+ T lymphocyte homeostasis by modulating O-glycan biosynthesis Immunity 12: 273–83 10755614.
20. Kaifu R, Osawa T, Jeanloz RW (1975) Synthesis of 2-O-(2-acetamido-2-deoxy-beta-D-glucopyranosyl)-D-mannose, and its interaction with D-mannose-specific lectins Carbohydr Res 40: 111–7 1125946.
21. Shinkawa T, Nakamura K, Yamane N, Shoji-Hosaka E, Kanda Y, et al. (2003) The absence of fucose but not the presence of galactose or bisecting N-acetylglucosamine of human IgG1 complex-type oligosaccharides shows the critical role of enhancing antibody-dependent cellular cytotoxicity J Biol Chem 278: 3466–73 12427744.
22. Wang X, Inoue S, Gu J, Miyoshi E, Noda K, et al. (2005) Dysregulation of TGF-beta1 receptor activation leads to abnormal lung development and emphysema-like phenotype in core fucose-deficient mice Proc Natl Acad Sci U S A 102: 15791–6 16236725.
23. Matsumoto I, Osawa T (1969) Purification and characterization of an anti-H(O) phytohemagglutinin of Ulex europeus Biochim Biophys Acta 194: 180–9 5353123.
24. Okajima T, Fukumoto S, Miyazaki H, Ishida H, Kiso M, et al. (1999) Molecular cloning of a novel alpha2,3-sialyltransferase (ST3Gal VI) that sialylates type II lactosamine structures on glycoproteins and glycolipids J Biol Chem 274: 11479–86 10206952.
25. Ito N, Imai S, Haga S, Nagaike C, Morimura Y, et al. (1996) Localization of binding sites of Ulex europaeus I, Helix pomatia and Griffonia simplicifolia I-B4 lectins and analysis of their backbone structures by several glycosidases and poly-N-acetyllactosamine-specific lectins in human breast carcinomas Histochem Cell Biol 106: 331–9 8897074.
26. Furukawa K, Sato T (1999) Beta-1,4-galactosylation of N-glycans is a complex process Biochim Biophys Acta 1473: 54–66 10580129.
27. Crowley JF, Goldstein IJ, Arnarp J, Lonngren J (1984) Carbohydrate binding studies on the lectin from Datura stramonium seeds Arch Biochem Biophys 231: 524–33 6203486.
28. Yamashita K, Totani K, Ohkura T, Takasaki S, Goldstein IJ, et al. (1987) Carbohydrate binding properties of complex-type oligosaccharides on immobilized Datura stramonium lectin J Biol Chem 262: 1602–7 3805046.
29. Ihara Y, Nishikawa A, Taniguchi N (1995) Effects of dibutyryl cAMP and bromodeoxyuridine on expression of N-acetylglucosaminyltransferases III and V in GOTO neuroblastoma cells Glycoconj J 12: 787–94 8748156.
30. Sasai K, Ikeda Y, Eguchi H, Tsuda T, Honke K, et al. (2002) The action of N-acetylglucosaminyltransferase-V is prevented by the bisecting GlcNAc residue at the catalytic step FEBS Lett 522: 151–5 12095636.
31. Miyoshi E, Nishikawa A, Ihara Y, Hayashi N, Fusamoto H, et al. (1994) Selective suppression of N-acetylglucosaminyltransferase III activity in a human hepatoblastoma cell line transfected with hepatitis B virus Cancer Res 54: 1854–8 8137300.
32. Sultan AS, Miyoshi E, Ihara Y, Nishikawa A, Tsukada Y, et al. (1997) Bisecting GlcNAc structures act as negative sorting signals for cell surface glycoproteins in forskolin-treated rat hepatoma cells J Biol Chem 272: 2866–72 9006930.
33. Wang WC, Cummings RD (1988) The immobilized leukoagglutinin from the seeds of Maackia amurensis binds with high affinity to complex-type Asn-linked oligosaccharides containing terminal sialic acid-linked alpha-2,3 to penultimate galactose residues J Biol Chem 263: 4576–85 3350806.
34. Konami Y, Yamamoto K, Osawa T, Irimura T (1994) Strong affinity of Maackia amurensis hemagglutinin (MAH) for sialic acid-containing Ser/Thr-linked carbohydrate chains of N-terminal octapeptides from human glycophorin A FEBS Lett 342: 334–8 8150094.
35. Knibbs RN, Goldstein IJ, Ratcliffe RM, Shibuya N (1991) Characterization of the carbohydrate binding specificity of the leukoagglutinating lectin from Maackia amurensis. Comparison with other sialic acid-specific lectins J Biol Chem 266: 83–8 1985926.

36. Stanley P, Caillibot V, Siminovitch L (1975) Selection and characterization of eight phenotypically distinct lines of lectin-resistant Chinese hamster ovary cell Cell 6: 121–8 1182798.
37. Kitagawa H, Paulson JC (1994) Differential expression of five sialyltransferase genes in human tissues J Biol Chem 269: 17872–8 8027041.
38. Bierhuizen MF, Mattei MG, Fukuda M (1993) Expression of the developmental I antigen by a cloned human cDNA encoding a member of a beta-1,6-N-acetylglucosaminyltransferase gene family Genes Dev 7: 468–78 8449405.
39. Moremen KW (2002) Golgi alpha-mannosidase II deficiency in vertebrate systems: implications for asparagine-linked oligosaccharide processing in mammals Biochim Biophys Acta 1573: 225–35 12417404.
40. Chen Y, Jain RK, Chandrasekaran EV, Matta KL (1995) Use of sialylated or sulfated derivatives and acrylamide copolymers of Gal beta 1,3GalNAc alpha- and GalNAc alpha- to determine the specificities of blood group T- and Tn-specific lectins and the copolymers to measure anti-T and anti-Tn antibody levels in cancer patients Glycoconj J 12: 55–62 7795413.
41. Nakamura-Tsuruta S, Kominami J, Kuno A, Hirabayashi J (2006) Evidence that Agaricus bisporus agglutinin (ABA) has dual sugar-binding specificity Biochem Biophys Res Commun 347: 215–20 16824489.
42. Hakomori S (2004) Carbohydrate-to-carbohydrate interaction in basic cell biology: a brief overview Arch Biochem Biophys 426: 173–81 15158668.
43. Paulson JC, Blixt O, Collins BE (2006) Sweet spots in functional glycomics Nat Chem Biol 2: 238–48 16619023.
44. Fukui S, Feizi T, Galustian C, Lawson AM, Chai W (2002) Oligosaccharide microarrays for high-throughput detection and specificity assignments of carbohydrate-protein interactions Nat Biotechnol 20: 1011–7 12219077.
45. Blixt O, Head S, Mondala T, Scanlan C, Huflejt ME, et al. (2004) Printed covalent glycan array for ligand profiling of diverse glycan binding proteins Proc Natl Acad Sci U S A 101: 17033–8 15563589.
46. Kamekawa N, Hayama K, Nakamura-Tsuruta S, Kuno A, Hirabayashi J (2006) A combined strategy for glycan profiling: a model study with pyridylaminated oligosaccharides J Biochem (Tokyo) 140: 337–47 16861248.
47. Edwards D (2003) Non-linear normalization and background correction in one-channel cDNA microarray studies Bioinformatics 19: 825–33 12724292.
48. Smyth GK (2005) Limma: linear models for microarray data. In: R. Gentleman VC, S. Dudoit, R. Irizarry, W. Huber, eds. 'Bioinformatics and Computational Biology Solutions using R and Bioconductor'. New York: Springer. pp Chapter 23.
49. Team RDC (2004) R: A Language and Environment for Statistical Computing. Vienna: R Foundation for Statistical Computing, http://www.R-project.org.
50. Morita S, Kojima T, Kitamura T (2000) Plat-E: An efficient and stable system for transient packaging of retroviruses Gene Ther 7: 1063–6 10871756.
51. Cummings R (1999) Plant Lectins. In: Varki A, Cummings R, Esko JD, Freeze HH, Hart GW, Marth J. Essentials of Glycobiology. New York: Cold Spring Harbor Laboratory Press. pp 455–468.

資料編1

シソーラスツリー

T1～T170ページ

- 解剖，生物名，病名，物質名を表す17,888語の日英併記の統制語について，最大10層のツリーに割り当てた。1つの統制語が複数のツリー下に属するため，全体でツリー項目数は36,185である。

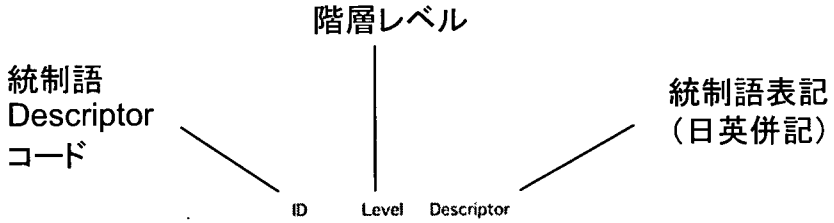

ID	Level	Descriptor
D001829	0	身体領域 Body Region
D000005	1	腹部 Abdomen
D034841	2	腹腔 Abdominal Cavity
D010537	3	腹膜 Peritoneum
D004312	4	ダグラス窩 Douglas' Pouch
D008643	4	腸間膜 Mesentery
D008646	5	結腸間膜 Mesocolon
D009852	4	網 Omentum
D010529	4	腹膜腔 Peritoneal Cavity
D054048	4	腹部ストーマ Peritoneal Stoma
D012187	3	後腹膜腔 Retroperitoneal Space
D034861	2	腹壁 Abdominal Wall
D006119	2	鼠径部 Groin
D007264	2	鼠径管 Inguinal Canal
D014472	2	臍 Umbilicus
D001415	1	背中 Back
D008161	2	腰仙部 Lumbosacral Region
D012445	2	仙尾骨部 Sacrococcygeal Region
D001940	1	乳房 Breast
D042361	2	ヒト乳腺 Human Mammary Gland
D009558	2	乳頭 Nipple
D005121	1	四肢 Extremities
D000672	2	切断端 Amputation Stump
D035002	2	下肢 Lower Extremity
D002081	3	殿部 Buttock
D005528	3	足 Foot
D000842	4	足首 Ankle
D005545	4	ヒト足先 Human Forefoot
D008684	5	中足 Metatarsus
D014034	5	つま先 Toe
D006214	6	母趾 Hallux
D006365	4	踵 Heel
D006615	3	尻 Hip
D007717	3	膝 Knee
D007866	3	脚 Leg
D013848	3	大腿 Thigh
D034941	2	上肢 Upper Extremity
D001132	3	腕 Arm
D001365	3	腋窩 Axilla
D004550	3	肘 Elbow
D005542	3	前腕 Forearm
D006225	3	手 Hand
D005385	4	手指 Finger
D013933	5	おや指 Thumb
D008663	4	中手 Metacarpus
D014953	4	手首 Wrist
D012782	3	肩 Shoulder

ID	Level	Descriptor
D001829	0	身体領域 Body Region
D000005	1	腹部 Abdomen
D034841	2	腹腔 Abdominal Cavity
D010537	3	腹膜 Peritoneum
D004312	4	ダグラス窩 Douglas' Pouch
D008643	4	腸間膜 Mesentery
D008646	5	結腸間膜 Mesocolon
D009852	4	網 Omentum
D010529	4	腹膜腔 Peritoneal Cavity
D054048	4	腹部ストーマ Peritoneal Stoma
D012187	3	後腹膜腔 Retroperitoneal Space
D034861	2	腹壁 Abdominal Wall
D006119	2	鼠径部 Groin
D007264	2	鼠径管 Inguinal Canal
D014472	2	臍 Umbilicus
D001415	1	背中 Back
D008161	2	腰仙部 Lumbosacral Region
D012445	2	仙尾骨部 Sacrococcygeal Region
D001940	1	乳房 Breast
D042361	2	ヒト乳腺 Human Mammary Gland
D009558	2	乳頭 Nipple
D005121	1	四肢 Extremities
D000672	2	切断端 Amputation Stump
D035002	2	下肢 Lower Extremity
D002081	3	殿部 Buttock
D005528	3	足 Foot
D000842	4	足首 Ankle
D005545	4	ヒト足先 Human Forefoot
D008684	5	中足 Metatarsus
D014034	5	つま先 Toe
D006214	6	母趾 Hallux
D006365	4	踵 Heel
D006615	3	尻 Hip
D007717	3	膝 Knee
D007866	3	脚 Leg
D013848	3	大腿 Thigh
D034941	2	上肢 Upper Extremity
D001132	3	腕 Arm
D001365	3	腋窩 Axilla
D004550	3	肘 Elbow
D005542	3	前腕 Forearm
D006225	3	手 Hand
D005385	4	手指 Finger
D013933	5	おや指 Thumb
D008663	4	中手 Metacarpus
D014953	4	手首 Wrist
D012782	3	肩 Shoulder
D006257	1	頭部 Head
D004423	2	耳 Ear
D005145	2	顔面 Face
D002610	3	頬 Cheek
D002680	3	頤 Chin
D005123	3	眼 Eye
D005138	4	眉 Eyebrow
D005143	4	眼瞼 Eyelid
D005140	5	睫毛 Eyelash
D005546	3	前頭 Forehead
D009055	3	口 Mouth
D008046	4	唇 Lip
D009666	3	鼻 Nose
D035421	3	耳下腺部 Parotid Region
D012535	2	頭皮 Scalp
D019291	2	頭蓋底 Skull Base
D035262	3	前頭蓋窩 Anterior Cranial Fossa
D035301	3	中頭蓋窩 Middle Cranial Fossa
D003388	3	後頭蓋窩 Posterior Cranial Fossa
D009333	1	首 Neck
D010388	1	骨盤 Pelvis
D017773	2	骨盤底 Pelvic Floor
D010502	1	会陰 Perineum
D013909	1	胸部 Thorax
D035423	2	胸腔 Thoracic Cavity
D008482	3	縦隔 Mediastinum
D035422	3	胸膜腔 Pleural Cavity
D035441	2	胸壁 Thoracic Wall
D014781	1	内臓 Viscera
D009141	0	筋骨格系 Musculoskeletal System
D002356	1	軟骨 Cartilage
D051472	2	弾性軟骨 Elastic Cartilage
D004425	3	耳介軟骨 Ear Cartilage
D007817	3	喉頭軟骨 Laryngeal Cartilage
D001193	4	披裂軟骨 Arytenoid Cartilage
D003413	4	輪状軟骨 Cricoid Cartilage
D004825	4	喉頭蓋 Epiglottis
D013957	4	甲状軟骨 Thyroid Cartilage
D051445	2	線維軟骨 Fibrocartilage
D007403	3	椎間板 Intervertebral Disk
D008592	3	脛骨半月 Tibial Meniscus
D051478	3	三角線維軟骨 Triangular Fibrocartilage
D051457	2	硝子軟骨 Hyaline Cartilage
D002358	3	関節軟骨 Articular Cartilage
D007817	3	喉頭軟骨 Laryngeal Cartilage
D001193	4	披裂軟骨 Arytenoid Cartilage
D003413	4	輪状軟骨 Cricoid Cartilage
D004825	4	喉頭蓋 Epiglottis
D013957	4	甲状軟骨 Thyroid Cartilage
D009300	3	鼻中隔 Nasal Septum
D005205	1	筋膜 Fascia
D005206	2	大腿筋膜 Fascia Lata
D008022	1	靭帯 Ligament
D001956	2	子宮広間膜 Broad Ligament
D008023	2	関節靭帯 Articular Ligament
D016118	3	前十字靭帯 Anterior Cruciate Ligament
D017885	3	側副靭帯 Collateral Ligament
D017844	4	外側靭帯 Ankle Lateral Ligament
D017888	4	膝内側側副靭帯 Knee Medial Collateral Ligament
D017846	3	縦靭帯 Longitudinal Ligament
D017847	3	膝蓋靭帯 Patellar Ligament
D016119	3	後十字靭帯 Posterior Cruciate Ligament
D012404	2	子宮円索 Round Ligament
D009132	1	筋肉 Muscle
D018485	2	筋線維 Muscle Fiber
D018656	3	速筋線維 Fast-Twitch Muscle Fiber
D018657	3	遅筋線維 Slow-Twitch Muscle Fiber
D009210	3	筋原線維 Myofibril
D012518	4	筋節 Sarcomere
D018482	2	骨格筋 Skeletal Muscle
D000009	3	腹筋 Abdominal Muscle
D017773	4	骨盤底 Pelvic Floor
D017568	4	腹直筋 Rectus Abdominis
D005152	3	顔面筋 Facial Muscle
D007821	3	喉頭筋 Laryngeal Muscle
D008410	3	咀嚼筋 Masticatory Muscle
D008406	4	咬筋 Masseter Muscle
D011626	4	翼状筋 Pterygoid Muscle
D013703	4	側頭筋 Temporal Muscle
D009334	3	頚筋 Neck Muscle
D009801	3	眼球運動筋 Oculomotor Muscle
D010156	3	口蓋筋 Palatal Muscle
D010369	3	胸筋 Pectoralis Muscle
D010609	3	咽頭筋 Pharyngeal Muscle
D049631	4	上部食道括約筋 Upper Esophageal Sphincter
D016658	3	腰筋 Psoas Muscle
D052097	3	四頭筋 Quadriceps Muscle
D012132	3	呼吸筋 Respiratory Muscle
D003964	4	横隔膜 Diaphragm
D007366	4	肋間筋 Intercostal Muscle
D017006	3	回旋筋腱板 Rotator Cuff
D012519	3	筋小胞体 Sarcoplasmic Reticulum
D013198	3	アブミ骨筋 Stapedius
D013719	3	鼓膜張筋 Tensor Tympani
D009130	2	平滑筋 Smooth Muscle
D049630	3	下部食道括約筋 Lower Esophageal Sphincter
D009131	3	血管平滑筋 Vascular Smooth Muscle
D017540	4	中膜 Tunica Media
D009215	3	子宮筋 Myometrium
D009206	2	心筋 Myocardium
D032386	3	心筋芽細胞 Cardiac Myoblast
D032383	3	心筋細胞 Cardiac Myocyte
D010210	3	乳頭筋 Papillary Muscle
D012863	1	骨格 Skeleton
D001842	2	骨 Bone
D050281	3	下肢骨 Bones of Lower Extremity
D005529	4	足骨 Foot Bone
D008682	5	中足骨 Metatarsal Bone
D013639	5	足根骨 Tarsal Bone
D002111	6	踵骨 Calcaneus
D013628	6	距骨 Talus
D050277	5	足指骨 Toe Phalanges
D007867	4	脚骨 Leg Bone
D005269	5	大腿骨 Femur
D005270	6	大腿骨頭 Femur Head
D005272	6	大腿骨頚 Femur Neck
D005360	5	腓骨 Fibula
D010329	5	膝蓋骨 Patella
D013977	5	脛骨 Tibia
D010384	4	骨盤 Pelvic Bone
D000077	5	寛骨臼 Acetabulum
D007085	5	腸骨 Ilium
D007512	5	坐骨 Ischium
D011630	5	恥骨 Pubic Bone
D001133	3	上肢骨 Bones of Upper Extremity
D050280	4	腕骨 Arm Bone
D006811	5	上腕骨 Humerus
D011884	5	橈骨 Radius
D014457	5	尺骨 Ulna
D002968	4	鎖骨 Clavicle
D050276	4	手骨 Hand Bone
D002348	5	手根骨 Carpal Bone
D051224	6	有頭骨 Capitate Bone
D051225	6	有鉤骨 Hamate Bone
D012667	6	月状骨 Lunate Bone
D051220	6	豆状骨 Pisiform Bone
D021361	6	舟状骨 Scaphoid Bone
D051222	6	大菱形骨 Trapezium Bone
D051223	6	小菱形骨 Trapezoid Bone
D051221	6	三角骨 Triquetrum Bone
D050278	5	指骨 Finger Phalanges
D050279	5	中手骨 Metacarpal Bone
D012540	4	肩甲骨 Scapula
D000174	5	肩峰 Acromion
D018483	3	骨幹 Diaphysis
D004838	3	骨端 Epiphysis
D006132	4	成長板 Growth Plate
D006928	3	舌骨 Hyoid Bone
D012716	3	種子骨 Sesamoid Bone
D012886	3	頭蓋骨 Skull
D003393	4	頭蓋縫合 Cranial Suture
D005004	4	篩骨 Ethmoid Bone
D005147	4	顔面骨 Facial Bone
D007568	5	下顎 Jaw
D000539	6	歯槽突起 Alveolar Process
D020390	7	歯槽 Tooth Socket
D003724	6	歯列弓 Dental Arch
D008334	6	下顎骨 Mandible
D002680	7	頤 Chin
D008335	7	下顎骨関節突起 Mandibular Condyle
D008437	6	上顎骨 Maxilla
D021362	6	硬口蓋 Hard Palate
D009295	5	鼻骨 Nasal Bone
D009915	5	眼窩 Orbit
D014420	5	鼻甲介 Turbinate

ID	Level	Descriptor
D005624	4	前頭骨 Frontal Bone
D009777	4	後頭骨 Occipital Bone
D005539	5	大後頭孔 Foramen Magnum
D010294	4	頭頂骨 Parietal Bone
D019291	4	頭蓋底 Skull Base
D035262	5	前頭蓋窩 Anterior Cranial Fossa
D035301	5	中頭蓋窩 Middle Cranial Fossa
D003388	5	後頭蓋窩 Posterior Cranial Fossa
D013100	4	蝶形骨 Sphenoid Bone
D012658	5	トルコ鞍 Sella Turcica
D013701	4	側頭骨 Temporal Bone
D008416	5	乳様突起 Mastoid
D010579	5	錐体骨 Petrous Bone
D013131	3	脊椎 Spine
D002574	4	頸椎 Cervical Vertebrae
D001270	5	環椎 Atlas
D001368	5	軸 Axis
D009809	6	歯突起 Odontoid Process
D003050	4	尾骨 Coccyx
D007403	4	椎間板 Intervertebral Disk
D008159	4	腰椎 Lumbar Vertebrae
D012447	4	仙骨 Sacrum
D013115	4	脊柱管 Spinal Canal
D004824	5	硬膜外腔 Epidural Space
D013904	4	胸椎 Thoracic Vertebrae
D013909	3	胸部 Thorax
D012272	4	肋骨 Rib
D013249	4	胸骨 Sternum
D008371	5	胸骨柄 Manubrium
D014989	5	剣状骨 Xiphoid Bone
D007596	2	関節 Joint
D000173	3	肩鎖関節 Acromioclavicular Joint
D001268	3	環軸関節 Atlanto-Axial Joint
D001269	3	環椎後頭関節 Atlanto-Occipital Joint
D002061	3	滑液包 Synovial Bursa
D002358	3	関節軟骨 Articular Cartilage
D004551	3	肘関節 Elbow Joint
D033023	3	足関節 Foot Joint
D000843	4	足首関節 Ankle Joint
D008683	4	中足指節関節 Metatarsophalangeal Joint
D013640	4	足根関節 Tarsal Joint
D013380	5	距骨下関節 Subtalar Joint
D014033	4	つま先関節 Toe Joint
D050823	3	手関節 Hand Joint
D050824	4	手根関節 Carpal Joint
D052737	4	手根中手関節 Carpometacarpal Joint
D005384	4	指関節 Finger Joint
D008662	4	中手指節関節 Metacarpophalangeal Joint
D053401	5	掌側板 Volar Plate
D014955	4	手首関節 Wrist Joint
D051478	5	三角線維軟骨 Triangular Fibrocartilage
D006621	3	股関節 Hip Joint
D017746	3	関節包 Joint Capsule
D013583	4	滑膜 Synovial Membrane
D013582	5	滑液 Synovial Fluid
D007719	3	膝関節 Knee Joint
D008592	4	脛骨半月 Tibial Meniscus
D008023	3	関節靱帯 Articular Ligament
D016118	4	前十字靱帯 Anterior Cruciate Ligament
D017885	4	側副靱帯 Collateral Ligament
D017844	5	外側靱帯 Ankle Lateral Ligament
D017888	5	膝内側側副靱帯 Knee Medial Collateral Ligament
D017843	4	黄色靱帯 Ligamentum Flavum
D017846	4	縦靱帯 Longitudinal Ligament
D017847	4	膝蓋靱帯 Patellar Ligament
D016119	4	後十字靱帯 Posterior Cruciate Ligament
D053401	4	掌側板 Volar Plate
D011631	3	恥骨結合 Pubic Symphysis
D012446	3	仙腸関節 Sacroiliac Joint
D012785	3	肩関節 Shoulder Joint
D013247	3	胸鎖関節 Sternoclavicular Joint
D013248	3	胸肋関節 Sternocostal Joint
D013704	3	顎関節 Temporomandibular Joint
D019224	4	顎関節円盤 Temporomandibular Joint Disk
D021801	3	関節突起間関節 Zygapophyseal Joint
D013710	1	腱 Tendon
D000125	2	アキレス腱 Achilles Tendon
D017847	2	膝蓋靱帯 Patellar Ligament
D017006	2	回旋筋腱板 Rotator Cuff
D004064	0	消化器系 Digestive System
D001659	1	胆道系 Biliary Tract
D001652	2	胆管 Bile Duct
D017734	3	肝外胆管 Extrahepatic Bile Duct
D003135	4	総胆管 Common Bile Duct
D014670	5	ファーター膨大部 Ampulla of Vater
D009803	6	オディ括約筋 Sphincter of Oddi
D003549	4	胆嚢管 Cystic Duct
D006500	4	総肝管 Common Hepatic Duct
D001653	3	肝内胆管 Intrahepatic Bile Duct
D001648	4	毛細胆管 Bile Canaliculi
D005704	2	胆嚢 Gallbladder
D041981	1	胃腸管 Gastrointestinal Tract
D007422	2	腸 Intestine
D007413	3	腸管粘膜 Intestinal Mucosa
D020895	4	腸細胞 Enterocyte
D020397	4	杯状細胞 Goblet Cell
D019879	4	パネート細胞 Paneth Cell
D007420	3	大腸 Large Intestine
D001003	4	肛門管 Anal Canal
D002432	4	盲腸 Cecum
D001065	5	虫垂 Appendix
D003106	4	結腸 Colon
D044682	5	上行結腸 Ascending Colon
D044683	5	下行結腸 Descending Colon
D012809	5	S状結腸 Sigmoid Colon
D044684	5	横行結腸 Transverse Colon
D007421	3	小腸 Small Intestine
D004386	4	十二指腸 Duodenum
D014670	5	ファーター膨大部 Ampulla of Vater
D009803	6	オディ括約筋 Sphincter of Oddi
D002011	5	ブルンネル腺 Brunner Gland
D007082	4	回腸 Ileum
D007080	5	回盲弁 Ileocecal Valve
D008467	5	メッケル憩室 Meckel Diverticulum
D007583	4	空腸 Jejunum
D041741	2	下部消化管 Lower Gastrointestinal Tract
D007082	3	回腸 Ileum
D007080	4	回盲弁 Ileocecal Valve
D008467	4	メッケル憩室 Meckel Diverticulum
D007420	3	大腸 Large Intestine
D001003	4	肛門管 Anal Canal
D002432	4	盲腸 Cecum
D001065	5	虫垂 Appendix
D003106	4	結腸 Colon
D044682	5	上行結腸 Ascending Colon
D044683	5	下行結腸 Descending Colon
D012809	5	S状結腸 Sigmoid Colon
D044684	5	横行結腸 Transverse Colon
D012007	4	直腸 Rectum
D007583	3	空腸 Jejunum
D009055	2	口 Mouth
D003817	3	歯列 Dentition
D012469	3	唾液腺 Salivary Gland
D010306	4	耳下腺 Parotid Gland
D018987	4	唾液腺管 Salivary Duct
D012470	4	小唾液腺 Minor Salivary Gland
D013361	4	舌下腺 Sublingual Gland
D013363	4	顎下腺 Submandibular Gland
D054838	4	フォンエブネル腺 Von Ebner Gland
D014059	3	舌 Tongue
D008035	4	舌小帯 Lingual Frenum
D013650	4	味蕾 Taste Bud
D010614	2	咽頭 Pharynx
D041742	2	上部消化管 Upper Gastrointestinal Tract
D004386	3	十二指腸 Duodenum
D014670	4	ファーター膨大部 Ampulla of Vater
D009803	5	オディ括約筋 Sphincter of Oddi
D002011	4	ブルンネル腺 Brunner Gland
D004947	3	食道 Esophagus
D049631	4	上部食道括約筋 Upper Esophageal Sphincter
D004943	4	食道胃接合部 Esophagogastric Junction
D049630	5	下部食道括約筋 Lower Esophageal Sphincter
D013270	3	胃 Stomach
D002299	4	噴門 Cardia
D004943	4	食道胃接合部 Esophagogastric Junction
D049630	5	下部食道括約筋 Lower Esophageal Sphincter
D005748	4	胃底部 Gastric Fundus
D005753	4	胃粘膜 Gastric Mucosa
D019872	5	胃主細胞 Gastric Chief Cell
D004759	5	腸クロマフィン細胞 Enterochromaffin Cell
D019863	5	ガストリン分泌細胞 Gastrin-Secreting Cell
D010295	5	胃壁細胞 Gastric Parietal Cell
D019864	5	ソマトスタチン分泌細胞 Somatostatin-Secreting Cell
D018530	4	胃断端 Gastric Stump
D011706	4	幽門洞 Pyloric Antrum
D011708	4	幽門 Pylorus
D008099	1	肝臓 Liver
D001653	2	肝内胆管 Intrahepatic Bile Duct
D001648	3	毛細胆管 Bile Canaliculi
D010179	1	膵臓 Pancreas
D007515	2	ランゲルハンス島 Islets of Langerhans
D050416	3	グルカゴン分泌細胞 Glucagon-Secreting Cell
D050417	3	インスリン分泌細胞 Insulin-Secreting Cell
D050418	3	膵臓ポリペプチド分泌細胞 Pancreatic Polypeptide-Secreting Cell
D019864	3	ソマトスタチン分泌細胞 Somatostatin-Secreting Cell
D046790	2	膵外分泌部 Exocrine Pancreas
D010183	2	膵管 Pancreatic Duct
D012137	0	呼吸器系 Respiratory System
D007830	1	喉頭 Larynx
D005931	2	声門 Glottis
D014827	3	声帯 Vocal Cord
D007817	2	喉頭軟骨 Laryngeal Cartilage
D001193	3	披裂軟骨 Arytenoid Cartilage
D003413	3	輪状軟骨 Cricoid Cartilage
D004825	3	喉頭蓋 Epiglottis
D013957	3	甲状軟骨 Thyroid Cartilage
D007820	2	喉頭粘膜 Laryngeal Mucosa
D020397	3	杯状細胞 Goblet Cell
D007821	2	喉頭筋 Laryngeal Muscle
D008168	1	肺 Lung
D001980	2	気管支 Bronchus
D015633	2	血管外肺水分 Extravascular Lung Water
D011650	2	肺胞 Pulmonary Alveoli
D015824	3	血液空気関門 Blood-Air Barrier
D009666	1	鼻 Nose
D009295	2	鼻骨 Nasal Bone
D009296	2	鼻腔 Nasal Cavity
D009297	2	鼻粘膜 Nasal Mucosa
D020397	3	杯状細胞 Goblet Cell
D009831	3	嗅粘膜 Olfactory Mucosa
D018034	4	嗅覚受容神経 Olfactory Receptor Neuron
D009300	2	鼻中隔 Nasal Septum
D019147	3	鋤鼻器官 Vomeronasal Organ
D010256	2	副鼻腔 Paranasal Sinus
D005005	3	篩骨洞 Ethmoid Sinus
D005626	3	前頭洞 Frontal Sinus
D008443	3	上顎洞 Maxillary Sinus
D013101	3	蝶形骨洞 Sphenoid Sinus
D014420	2	鼻甲介 Turbinate
D010614	1	咽頭 Pharynx
D007013	2	下咽頭 Hypopharynx
D009305	2	上咽頭 Nasopharynx

ID	Level	Descriptor
D014066	3	扁桃腺 Tonsil
D010609	2	咽頭筋 Pharyngeal Muscle
D049631	3	上部食道括約筋 Upper Esophageal Sphincter
D010994	1	胸膜 Pleura
D020545	1	呼吸粘膜 Respiratory Mucosa
D020397	2	杯状細胞 Goblet Cell
D007820	2	喉頭粘膜 Laryngeal Mucosa
D009297	2	鼻粘膜 Nasal Mucosa
D009831	3	嗅粘膜 Olfactory Mucosa
D018034	4	嗅覚受容神経 Olfactory Receptor Neuron
D014132	1	気管 Trachea
D014566	0	泌尿生殖器系 Urogenital System
D005835	1	生殖器 Genitalia
D005836	2	女性生殖器 Female Genitalia
D000290	3	子宮付属器 Adnexa Uteri
D001956	4	子宮広間膜 Broad Ligament
D005187	4	卵管 Fallopian Tube
D010053	4	卵巣 Ovary
D003338	5	黄体 Corpus Luteum
D008184	6	黄体細胞 Luteal Cell
D006080	5	卵胞 Ovarian Follicle
D015571	6	卵胞液 Follicular Fluid
D006107	6	顆粒膜細胞 Granulosa Cell
D054885	7	卵丘細胞 Cumulus Cell
D013799	6	卵胞膜細胞 Theca Cell
D012404	4	子宮円索 Round Ligament
D014599	3	子宮 Uterus
D002584	4	子宮頚部 Cervix Uteri
D004717	4	子宮内膜 Endometrium
D003656	5	脱落膜 Decidua
D033301	6	脱落膜腫 Deciduoma
D009215	4	子宮筋 Myometrium
D014621	3	腟 Vagina
D006924	4	処女膜 Hymen
D014844	3	外陰部 Vulva
D001472	4	バルトリン腺 Bartholin's Gland
D002987	4	陰核 Clitoris
D005837	2	男性生殖器 Male Genitalia
D002030	3	尿道球腺 Bulbourethral Gland
D004543	3	射精管 Ejaculatory Duct
D004822	3	精巣上体 Epididymis
D010413	3	陰茎 Penis
D052816	4	包皮 Foreskin
D014521	4	尿道 Urethra
D011467	3	前立腺 Prostate
D012611	3	陰嚢 Scrotum
D012669	3	精嚢 Seminal Vesicle
D013085	3	精索 Spermatic Cord
D013737	3	精巣 Testis
D007985	4	ライディッヒ細胞 Leydig Cell
D012152	4	精巣網 Rete Testis
D012671	4	精細管 Seminiferous Tubule
D001814	5	血液精巣関門 Blood-Testis Barrier
D012670	5	精上皮 Seminiferous Epithelium
D012708	4	セルトリ細胞 Sertoli Cell
D014649	3	輸精管 Vas Deferens
D005854	2	生殖細胞 Germ Cell
D010063	3	卵子 Ovum
D009865	4	卵母細胞 Oocyte
D009867	4	卵原細胞 Oogonia
D015044	4	透明帯 Zona Pellucida
D015053	4	接合体 Zygote
D013094	3	精子 Spermatozoa
D013077	4	精子頭部 Sperm Head
D000177	5	先体 Acrosome
D032961	4	精子中間部 Sperm Midpiece
D013082	4	精子尾部 Sperm Tail
D013087	4	精細胞 Spermatid
D013090	4	精母細胞 Spermatocyte
D013093	4	精原細胞 Spermatogonia
D006066	2	生殖腺 Gonad
D010053	3	卵巣 Ovary
D013737	3	精巣 Testis
D014551	1	尿路 Urinary Tract
D007668	2	腎臓 Kidney
D007672	3	腎皮質 Kidney Cortex
D007678	4	腎糸球体 Kidney Glomerulus
D050533	5	糸球体基底膜 Glomerular Basement Membrane
D007606	5	傍糸球体装置 Juxtaglomerular Apparatus
D050527	5	メサンギウム細胞 Mesangial Cell
D005920	6	糸球体間質 Glomerular Mesangium
D050199	5	有足細胞 Podocyte
D007679	3	腎髄質 Kidney Medulla
D007682	3	腎盂 Kidney Pelvis
D007670	4	腎杯 Kidney Calix
D009399	3	ネフロン Nephron
D007678	4	腎糸球体 Kidney Glomerulus
D050533	5	糸球体基底膜 Glomerular Basement Membrane
D007606	5	傍糸球体装置 Juxtaglomerular Apparatus
D050527	5	メサンギウム細胞 Mesangial Cell
D005920	6	糸球体間質 Glomerular Mesangium
D050199	5	有足細胞 Podocyte
D007684	4	腎尿細管 Kidney Tubule
D050476	5	ボーマン嚢 Bowman Capsule
D007685	5	集合管 Collecting Kidney Tubule
D007686	5	遠位尿細管 Distal Kidney Tubule
D007687	5	腎近位尿細管 Proximal Kidney Tubule
D008138	5	ヘンレ係蹄 Loop of Henle
D014513	2	尿管 Ureter
D014521	2	尿道 Urethra
D001743	2	膀胱 Urinary Bladder
D004703	0	内分泌系 Endocrine System
D002838	1	クロム親和系 Chromaffin System
D019439	2	クロム親和性細胞 Chromaffin Cell
D002837	3	クロマフィン顆粒 Chromaffin Granule
D004759	2	腸クロマフィン細胞 Enterochromaffin Cell
D010220	2	大動脈傍体 Para-Aortic Body
D010233	2	クロム親和性傍神経節 Chromaffin Paraganglia
D019858	1	腸管内分泌細胞 Enteroendocrine Cell
D004759	2	腸クロマフィン細胞 Enterochromaffin Cell
D019861	2	腸クロム親和性細胞様細胞 Enterochromaffin-like Cell
D019863	2	ガストリン分泌細胞 Gastrin-Secreting Cell
D050416	2	グルカゴン分泌細胞 Glucagon-Secreting Cell
D050417	2	インスリン分泌細胞 Insulin-Secreting Cell
D050418	2	膵臓ポリペプチド分泌細胞 Pancreatic Polypeptide-Secreting Cell
D019864	2	ソマトスタチン分泌細胞 Somatostatin-Secreting Cell
D004702	1	内分泌腺 Endocrine Gland
D000311	2	副腎 Adrenal Gland
D000302	3	副腎皮質 Adrenal Cortex
D015383	4	束状層 Zona Fasciculata
D015384	4	球状層 Zona Glomerulosa
D015385	4	網状層 Zona Reticularis
D000313	3	副腎髄質 Adrenal Medulla
D006066	2	生殖腺 Gonad
D010053	3	卵巣 Ovary
D003338	4	黄体 Corpus Luteum
D008184	5	黄体細胞 Luteal Cell
D006080	4	卵胞 Ovarian Follicle
D015571	5	卵胞液 Follicular Fluid
D006107	5	顆粒膜細胞 Granulosa Cell
D054885	6	卵丘細胞 Cumulus Cell
D013799	5	卵胞膜細胞 Theca Cell
D013737	3	精巣 Testis
D007985	4	ライディッヒ細胞 Leydig Cell
D007515	2	ランゲルハンス島 Islets of Langerhans
D050416	3	グルカゴン分泌細胞 Glucagon-Secreting Cell
D050417	3	インスリン分泌細胞 Insulin-Secreting Cell
D050418	3	膵臓ポリペプチド分泌細胞 Pancreatic Polypeptide-Secreting Cell
D019864	3	ソマトスタチン分泌細胞 Somatostatin-Secreting Cell
D010280	2	副甲状腺 Parathyroid Gland
D010870	2	松果体 Pineal Gland
D010913	2	下垂体副腎皮質系 Pituitary-Adrenal System
D010902	2	脳下垂体 Pituitary Gland
D010903	3	脳下垂体前葉 Anterior Pituitary Gland
D052680	4	副腎皮質刺激ホルモン分泌細胞 Corticotroph
D052681	4	性腺刺激ホルモン分泌細胞 Gonadotroph
D052682	4	乳腺刺激ホルモン分泌細胞 Lactotroph
D052683	4	成長ホルモン分泌細胞 Somatotroph
D052684	4	甲状腺刺激ホルモン分泌細胞 Thyrotroph
D052716	3	脳下垂体中葉 Intermediate Pituitary Gland
D052717	4	メラニン細胞刺激ホルモン産生細胞 Melanotroph
D010904	3	脳下垂体後葉 Posterior Pituitary Gland
D013961	2	甲状腺 Thyroid Gland
D009490	1	神経分泌系 Neurosecretory System
D007030	2	視床下部下垂体系 Hypothalamo-Hypophyseal System
D008473	3	正中隆起 Median Eminence
D010902	3	脳下垂体 Pituitary Gland
D010903	4	脳下垂体前葉 Anterior Pituitary Gland
D052680	5	副腎皮質刺激ホルモン分泌細胞 Corticotroph
D052681	5	性腺刺激ホルモン分泌細胞 Gonadotroph
D052682	5	乳腺刺激ホルモン分泌細胞 Lactotroph
D052683	5	成長ホルモン分泌細胞 Somatotroph
D052684	5	甲状腺刺激ホルモン分泌細胞 Thyrotroph
D052716	4	脳下垂体中葉 Intermediate Pituitary Gland
D052717	5	メラニン細胞刺激ホルモン産生細胞 Melanotroph
D010904	4	脳下垂体後葉 Posterior Pituitary Gland
D010870	2	松果体 Pineal Gland
D002319	0	循環器 Cardiovascular System
D015824	1	血液空気関門 Blood-Air Barrier
D018916	1	血液房水関門 Blood-Aqueous Barrier
D001812	1	血液脳関門 Blood-Brain Barrier
D049428	1	血液神経関門 Blood-Nerve Barrier
D001813	1	血液網膜関門 Blood-Retinal Barrier
D001814	1	血液精巣関門 Blood-Testis Barrier
D001808	1	血管 Blood Vessel
D001158	2	動脈 Artery
D001011	3	大動脈 Aorta
D001012	4	腹部大動脈 Abdominal Aorta
D001013	4	胸部大動脈 Thoracic Aorta
D012850	4	バルサルバ洞 Sinus of Valsalva
D001160	3	細動脈 Arteriole
D001366	3	腋窩動脈 Axillary Artery
D001488	3	脳底動脈 Basilar Artery
D001916	3	上腕動脈 Brachial Artery
D016122	3	腕頭動脈 Brachiocephalic Trunk
D001981	3	気管支動脈 Bronchial Artery
D002339	3	頚動脈 Carotid Artery
D017536	4	総頚動脈 Common Carotid Artery
D002342	5	外頚動脈 External Carotid Artery
D002343	5	内頚動脈 Internal Carotid Artery
D002346	4	頚動脈洞 Carotid Sinus
D002445	3	腹腔動脈 Celiac Artery
D002536	3	大脳動脈 Cerebral Artery
D020771	4	前大脳動脈 Anterior Cerebral Artery
D002941	4	ウィリス動脈輪 Circle of Willis
D020768	4	中大脳動脈 Middle Cerebral Artery
D020769	4	後大脳動脈 Posterior Cerebral Artery
D013699	4	側頭動脈 Temporal Artery
D019842	3	毛様体動脈 Ciliary Artery
D003331	3	冠血管 Coronary Vessel
D019074	3	腹壁動脈 Epigastric Artery
D005263	3	大腿動脈 Femoral Artery
D024405	3	胃大網動脈 Gastroepiploic Artery
D006499	3	総肝動脈 Hepatic Artery
D007083	3	腸骨動脈 Iliac Artery
D008438	3	顎動脈 Maxillary Artery
D008576	3	硬膜動脈 Meningeal Artery
D008638	3	腸間膜動脈 Mesenteric Artery
D017537	4	下腸間膜動脈 Inferior Mesenteric Artery
D017538	4	上腸間膜動脈 Superior Mesenteric Artery
D009880	3	眼動脈 Ophthalmic Artery
D011150	3	膝窩動脈 Popliteal Artery

ID	Level	Descriptor
D017534	3	橈骨動脈 Radial Artery
D012077	3	腎動脈 Renal Artery
D012161	3	網膜動脈 Retinal Artery
D013157	3	脾動脈 Splenic Artery
D013348	3	鎖骨下動脈 Subclavian Artery
D013895	3	胸動脈 Thoracic Artery
D008323	4	乳動脈 Mammary Artery
D016909	3	脛骨動脈 Tibial Artery
D017535	3	尺骨動脈 Ulnar Artery
D014469	3	臍帯動脈 Umbilical Artery
D014711	3	椎骨動脈 Vertebral Artery
D004730	2	血管内皮 Vascular Endothelium
D020286	3	周皮細胞 Pericyte
D017539	3	内膜 Tunica Intima
D008833	2	微小循環 Microcirculation
D001160	3	細動脈 Arteriole
D001163	3	動静脈吻合 Arteriovenous Anastomosis
D002196	3	毛細管 Capillary
D014699	3	細静脈 Venule
D009131	2	血管平滑筋 Vascular Smooth Muscle
D017540	3	中膜 Tunica Media
D012171	2	網膜血管 Retinal Vessel
D012161	3	網膜動脈 Retinal Artery
D012169	3	網膜静脈 Retinal Vein
D017539	2	内膜 Tunica Intima
D014650	2	神経栄養血管 Vasa Nervorum
D014651	2	脈管の脈管 Vasa Vasorum
D014680	2	静脈 Vein
D001367	3	腋窩静脈 Axillary Vein
D001401	3	奇静脈 Azygos Vein
D016121	3	腕頭静脈 Brachiocephalic Vein
D002550	3	大脳静脈 Cerebral Vein
D003331	3	冠血管 Coronary Vessel
D054326	4	冠静脈洞 Coronary Sinus
D003392	3	硬膜静脈洞 Cranial Sinus
D002426	4	海綿静脈洞 Cavernous Sinus
D054063	4	上矢状静脈洞 Superior Sagittal Sinus
D054064	4	横静脈洞 Transverse Sinus
D005268	3	大腿静脈 Femoral Vein
D006503	3	肝静脈 Hepatic Vein
D007084	3	腸骨静脈 Iliac Vein
D007601	3	頚静脈 Jugular Vein
D011152	3	膝窩静脈 Popliteal Vein
D011168	3	門脈系 Portal System
D008642	4	腸間膜静脈 Mesenteric Vein
D011169	4	門脈 Portal Vein
D013162	4	脾静脈 Splenic Vein
D014471	4	臍帯静脈 Umbilical Vein
D011667	3	肺静脈 Pulmonary Vein
D012082	3	腎静脈 Renal Vein
D012169	3	網膜静脈 Retinal Vein
D012501	3	伏在静脈 Saphenous Vein
D013350	3	鎖骨下静脈 Subclavian Vein
D014684	3	大静脈 Venae Cavae
D014682	4	下大静脈 Inferior Vena Cava
D014683	4	上大静脈 Superior Vena Cava
D014699	3	細静脈 Venule
D006321	1	心臓 Heart
D004699	2	心内膜 Endocardium
D005318	2	胎児心臓 Fetal Heart
D004373	3	動脈管 Ductus Arteriosus
D014338	3	総動脈幹 Truncus Arteriosus
D006325	2	心房 Heart Atria
D020517	3	心耳 Atrial Appendage
D006329	2	心臓刺激伝導系 Heart Conduction System
D001283	3	房室結節 Atrioventricular Node
D002036	3	ヒス束 Bundle of His
D011690	3	プルキンエ線維 Purkinje Fiber
D012849	3	洞房結節 Sinoatrial Node
D006346	2	心臓中隔 Heart Septum
D054087	3	心房中隔 Atrial Septum
D054089	3	心内膜床 Endocardial Cushion
D054085	3	卵円孔 Foramen Ovale
D054088	3	心室中隔 Ventricular Septum
D006351	2	心臓弁 Heart Valve
D001021	3	大動脈弁 Aortic Valve
D002815	3	腱索 Chordae Tendineae
D008943	3	僧帽弁 Mitral Valve
D010210	3	乳頭筋 Papillary Muscle
D011664	3	肺動脈弁 Pulmonary Valve
D014261	3	三尖弁 Tricuspid Valve
D006352	2	心室 Heart Ventricle
D009206	2	心筋 Myocardium
D032386	3	心筋芽細胞 Cardiac Myoblast
D032383	3	心筋細胞 Cardiac Myocyte
D010210	3	乳頭筋 Papillary Muscle
D010210	2	乳頭筋 Papillary Muscle
D010496	2	心膜 Pericardium
D009420	0	神経系 Nervous System
D002490	1	中枢神経系 Central Nervous System
D001921	2	脳 Brain
D001812	3	血液脳関門 Blood-Brain Barrier
D001933	3	脳幹 Brain Stem
D008636	4	中脳 Mesencephalon
D008125	5	青斑核 Locus Coeruleus
D011903	5	縫線核 Raphe Nucleus
D003336	5	中脳蓋 Tectum Mesencephali
D007245	6	下丘 Inferior Colliculi
D013477	6	上丘 Superior Colliculi
D013681	5	中脳被蓋 Tegmentum Mesencephali
D002535	6	中脳水道 Cerebral Aqueduct
D045042	6	橋脚被蓋核 Pedunculopontine Tegmental Nucleus
D010487	6	中脳水道周囲灰白質 Periaqueductal Gray
D012012	6	赤核 Red Nucleus
D013378	6	黒質 Substantia Nigra
D017557	6	腹側被蓋野 Ventral Tegmental Area
D012125	5	呼吸中枢 Respiratory Center
D012249	4	菱脳 Rhombencephalon
D008526	5	延髄 Medulla Oblongata
D031608	6	最後野 Area Postrema
D009847	6	オリーブ核 Olivary Nucleus
D017552	6	孤束核 Solitary Nucleus
D020540	5	後脳 Metencephalon
D002531	6	小脳 Cerebellum
D002525	7	小脳皮質 Cerebellar Cortex
D011689	8	プルキンエ細胞 Purkinje Cell
D002529	7	小脳核 Cerebellar Nucleus
D002530	7	小脳橋角 Cerebellopontine Angle
D011149	6	橋 Pons
D017626	7	蝸牛神経核 Cochlear Nucleus
D008125	7	青斑核 Locus Coeruleus
D014726	7	前庭神経核 Vestibular Nucleus
D003689	8	前庭神経外側核 Lateral Vestibular Nucleus
D011903	5	縫線核 Raphe Nucleus
D014278	4	三叉神経核 Trigeminal Nucleus
D014279	5	三叉神経脊髄路核 Spinal Trigeminal Nucleus
D014275	6	三叉神経尾側核 Trigeminal Caudal Nucleus
D002552	3	脳室 Cerebral Ventricle
D002535	4	中脳水道 Cerebral Aqueduct
D002831	4	脈絡叢 Choroid Plexus
D004805	4	上衣 Ependyma
D020546	4	第四脳室 Fourth Ventricle
D020547	4	側脳室 Lateral Ventricle
D012688	4	透明中隔 Septum Pellucidum
D020542	4	第三脳室 Third Ventricle
D008032	3	辺縁系 Limbic System
D000679	4	扁桃体 Amygdala
D019261	4	視床上部 Epithalamus
D019262	5	手綱 Habenula
D020712	4	脳弓 Brain Fornix
D006179	4	帯状回 Gyrus Cinguli
D006624	4	海馬 Hippocampus
D018891	5	歯状回 Dentate Gyrus
D019599	6	海馬苔状線維 Hippocampal Mossy Fiber
D017966	5	錐体細胞 Pyramidal Cell
D007031	4	視床下部 Hypothalamus
D009833	4	嗅覚経路 Olfactory Pathway
D020670	5	カジェハ島 Islands of Calleja
D009830	5	嗅球 Olfactory Bulb
D020534	4	海馬傍回 Parahippocampal Gyrus
D018728	5	嗅内皮質 Entorhinal Cortex
D020665	4	脳中隔 Septum of Brain
D012686	5	中隔核 Septal Nucleus
D013377	4	無名質 Substantia Innominata
D008636	3	中脳 Mesencephalon
D008125	4	青斑核 Locus Coeruleus
D011903	4	縫線核 Raphe Nucleus
D003336	4	中脳蓋 Tectum Mesencephali
D007245	5	下丘 Inferior Colliculi
D013477	5	上丘 Superior Colliculi
D013681	4	中脳被蓋 Tegmentum Mesencephali
D002535	5	中脳水道 Cerebral Aqueduct
D045042	5	橋脚被蓋核 Pedunculopontine Tegmental Nucleus
D010487	5	中脳水道周囲灰白質 Periaqueductal Gray
D012012	5	赤核 Red Nucleus
D013378	5	黒質 Substantia Nigra
D017557	5	腹側被蓋野 Ventral Tegmental Area
D016548	3	前脳 Prosencephalon
D004027	4	間脳 Diencephalon
D019261	5	視床上部 Epithalamus
D019262	6	手綱 Habenula
D010870	6	松果体 Pineal Gland
D007031	5	視床下部 Hypothalamus
D007026	6	視床下部外側野 Lateral Hypothalamic Area
D007032	6	視床下部前部 Anterior Hypothalamus
D007025	7	視床下部前核 Anterior Hypothalamic Nucleus
D010286	7	視床下部室傍核 Paraventricular Hypothalamic Nucleus
D011301	7	視索前野 Preoptic Area
D013493	7	視交叉上核 Suprachiasmatic Nucleus
D013495	7	視索上核 Supraoptic Nucleus
D007033	6	視床下部中間部 Middle Hypothalamus
D001111	7	弓状核 Arcuate Nucleus
D004302	7	視床下部背内側核 Dorsomedial Hypothalamic Nucleus
D007030	7	視床下部下垂体系 Hypothalamo-Hypophyseal System
D008473	8	正中隆起 Median Eminence
D010902	8	脳下垂体 Pituitary Gland
D010903	9	脳下垂体前葉 Anterior Pituitary Gland
D052680	10	副腎皮質刺激ホルモン分泌細胞 Corticotroph
D052681	10	性腺刺激ホルモン分泌細胞 Gonadotroph
D052682	10	乳腺刺激ホルモン分泌細胞 Lactotroph
D052683	10	成長ホルモン分泌細胞 Somatotroph
D052684	10	甲状腺刺激ホルモン分泌細胞 Thyrotroph
D052716	9	脳下垂体中葉 Intermediate Pituitary Gland
D052717	10	メラニン細胞刺激ホルモン産生細胞 Melanotroph
D010904	9	脳下垂体後葉 Posterior Pituitary Gland
D014371	7	灰白隆起 Tuber Cinereum
D014697	7	視床下部腹内側核 Ventromedial Hypothalamic Nucleus
D007034	6	視床下部後部 Posterior Hypothalamus
D008326	7	乳頭体 Mamillary Body
D020530	5	腹側視床 Subthalamus
D020392	6	脳脚内核 Entopeduncular Nucleus
D020531	6	視床下核 Subthalamic Nucleus
D013788	5	視床 Thalamus
D013787	6	視床核 Thalamic Nucleus
D020643	7	視床前核 Anterior Thalamic Nucleus
D005829	7	膝状体 Geniculate Body
D020646	7	視床髄板内核 Intralaminar Thalamic Nucleus
D020647	7	視床外側核 Lateral Thalamic Nucleus
D020649	8	視床枕 Pulvinar
D020645	7	視床背内側核 Mediodorsal Thalamic Nucleus
D020644	7	視床正中核 Midline Thalamic Nucleus
D020656	7	視床後核 Posterior Thalamic Nucleus

ID	Level	Descriptor
D013687	4	終脳 Telencephalon
D054022	5	大脳 Cerebrum
D001479	6	基底核 Basal Ganglia
D000679	7	扁桃体 Amygdala
D003342	7	線条体 Corpus Striatum
D005917	8	淡蒼球 Globus Pallidus
D017072	8	新線条体 Neostriatum
D002421	9	尾状核 Caudate Nucleus
D053400	9	高次発声中枢 High Vocal Center
D011699	9	被殻 Putamen
D009714	7	側坐核 Nucleus Accumbens
D013377	7	無名質 Substantia Innominata
D020532	8	マイネルト基底核 Basal Nucleus of Meynert
D002540	6	大脳皮質 Cerebral Cortex
D005625	7	前頭葉 Frontal Lobe
D009044	8	運動皮質 Motor Cortex
D017397	8	前頭前野 Prefrontal Cortex
D006624	7	海馬 Hippocampus
D018891	8	歯状回 Dentate Gyrus
D019599	9	海馬苔状線維 Hippocampal Mossy Fiber
D017966	8	錐体細胞 Pyramidal Cell
D019579	7	新皮質 Neocortex
D009778	7	後頭葉 Occipital Lobe
D014793	8	視覚野 Visual Cortex
D010296	7	頭頂葉 Parietal Lobe
D013003	8	体性感覚皮質 Somatosensory Cortex
D017966	7	錐体細胞 Pyramidal Cell
D013702	7	側頭葉 Temporal Lobe
D001303	8	聴覚皮質 Auditory Cortex
D020534	8	海馬傍回 Parahippocampal Gyrus
D018728	9	嗅内皮質 Entorhinal Cortex
D003337	5	脳梁 Corpus Callosum
D020667	5	ブローカ対角帯 Diagonal Band of Broca
D020712	5	脳弓 Brain Fornix
D020772	5	内包 Internal Capsule
D009833	5	嗅覚経路 Olfactory Pathway
D020670	6	カジェハ島 Islands of Calleja
D009830	6	嗅球 Olfactory Bulb
D020665	5	脳中隔 Septum of Brain
D012686	6	中隔核 Septal Nucleus
D012688	6	透明中隔 Septum Pellucidum
D012249	3	菱脳 Rhombencephalon
D020540	4	後脳 Metencephalon
D002531	5	小脳 Cerebellum
D002525	6	小脳皮質 Cerebellar Cortex
D011689	7	プルキンエ細胞 Purkinje Cell
D002529	6	小脳核 Cerebellar Nucleus
D002530	6	小脳橋角 Cerebellopontine Angle
D011149	5	橋 Pons
D017626	6	蝸牛神経核 Cochlear Nucleus
D008125	6	青斑核 Locus Coeruleus
D014726	6	前庭神経核 Vestibular Nucleus
D003689	7	前庭神経外側核 Lateral Vestibular Nucleus
D054024	4	髄脳 Myelencephalon
D008526	5	延髄 Medulla Oblongata
D031608	6	最後野 Area Postrema
D009847	6	オリーブ核 Olivary Nucleus
D017552	6	孤束核 Solitary Nucleus
D011903	4	縫線核 Raphe Nucleus
D008578	2	髄膜 Meninges
D001099	3	くも膜 Arachnoid
D013346	4	くも膜下腔 Subarachnoid Space
D002946	5	大槽 Cisterna Magna
D004388	3	硬膜 Dura Mater
D013355	4	硬膜下腔 Subdural Space
D010841	3	軟膜 Pia Mater
D013116	2	脊髄 Spinal Cord
D000870	3	前角細胞 Anterior Horn Cell
D005116	3	錐体外路 Extrapyramidal Tract
D020671	3	後角細胞 Posterior Horn Cell
D013376	4	膠様質 Substantia Gelatinosa
D011712	3	錐体路 Pyramidal Tract
D013133	3	脊髄視床路 Spinothalamic Tract
D005724	1	神経節 Ganglia
D005725	2	自律神経節 Autonomic Ganglia
D005726	3	副交感神経節 Parasympathetic Ganglia
D005728	3	交感神経節 Sympathetic Ganglia
D013233	4	星状神経節 Stellate Ganglion
D017783	4	上頚神経節 Superior Cervical Ganglion
D017952	2	無脊椎動物神経節 Invertebrate Ganglia
D017950	2	感覚神経節 Sensory Ganglia
D005727	3	脊髄神経節 Spinal Ganglion
D005830	3	膝神経節 Geniculate Ganglion
D009620	3	下神経節 Nodose Ganglion
D013136	3	らせん神経節 Spiral Ganglion
D012668	3	三叉神経節 Trigeminal Ganglion
D027161	2	ニューロン周囲サテライト細胞 Perineuronal Satellite Cell
D009415	1	神経網 Nerve Net
D009417	1	神経組織 Nerve Tissue
D004805	2	上衣 Ependyma
D009441	2	神経鞘 Neurilemma
D009434	1	神経路 Neural Pathway
D000344	2	求心路 Afferent Pathway
D001306	3	聴覚路 Auditory Pathway
D009833	3	嗅覚経路 Olfactory Pathway
D020824	3	脊髄小脳路 Spinocerebellar Tract
D013133	3	脊髄視床路 Spinothalamic Tract
D017833	3	自律神経求心路 Visceral Afferent
D014795	3	視覚路 Visual Pathway
D004525	2	遠心路 Efferent Pathway
D005116	3	錐体外路 Extrapyramidal Tract
D011712	3	錐体路 Pyramidal Tract
D020772	2	内包 Internal Capsule
D008474	2	内側前脳束 Medial Forebrain Bundle
D019580	2	貫通線維路 Perforant Pathway
D009457	1	神経膠細胞 Neuroglia
D017628	2	ミクログリア Microglia
D019581	2	ニューロパイル Neuropil
D019600	3	糸屑状構造物 Neuropil Thread
D009836	2	オリゴデンドログリア Oligodendroglia
D009186	3	髄鞘 Myelin Sheath
D027161	2	ニューロン周囲サテライト細胞 Perineuronal Satellite Cell
D012583	2	シュワン細胞 Schwann Cell
D009186	3	髄鞘 Myelin Sheath
D009441	4	神経鞘 Neurilemma
D011901	4	ランビエ絞輪 Ranvier's Node
D009474	1	ニューロン Neuron
D003712	2	樹状突起 Dendrite
D049229	3	樹状突起棘 Dendritic Spine
D016501	3	神経突起 Neurite
D020439	2	成長円錐 Growth Cone
D007395	2	介在ニューロン Interneuron
D025042	3	アマクリン細胞 Amacrine Cell
D051245	3	網膜双極細胞 Retinal Bipolar Cell
D016631	2	レビー小体 Lewy Body
D009412	2	神経線維 Nerve Fiber
D000320	3	アドレナリン作動性線維 Adrenergic Fiber
D017779	4	交感神経節後線維 Postganglionic Sympathetic Fiber
D001338	3	自律神経節後線維 Postganglionic Autonomic Fiber
D017777	4	副交感神経節後線維 Postganglionic Parasympathetic Fiber
D017779	4	交感神経節後線維 Postganglionic Sympathetic Fiber
D001339	3	自律神経節前線維 Preganglionic Autonomic Fiber
D001369	3	軸索 Axon
D016501	4	神経突起 Neurite
D017729	4	シナプス前終末 Presynaptic Terminal
D019599	5	海馬苔状線維 Hippocampal Mossy Fiber
D002799	3	コリン作動性線維 Cholinergic Fiber
D001339	4	自律神経節前線維 Preganglionic Autonomic Fiber
D017777	4	副交感神経節後線維 Postganglionic Parasympathetic Fiber
D009413	3	有髄神経線維 Myelinated Nerve Fiber
D009186	4	髄鞘 Myelin Sheath
D009441	5	神経鞘 Neurilemma
D011901	5	ランビエ絞輪 Ranvier's Node
D036421	3	無髄神経線維 Unmyelinated Nerve Fiber
D009430	2	ニューラルアナライザ Neural Analyzer
D009454	2	神経原線維 Neurofibril
D016874	3	神経原線維変化 Neurofibrillary Tangle
D009475	2	求心性ニューロン Afferent Neuron
D006198	3	聴覚有毛細胞 Auditory Hair Cell
D006199	4	内有毛細胞 Inner Auditory Hair Cell
D018072	4	外有毛細胞 Outer Auditory Hair Cell
D018069	3	前庭有毛細胞 Vestibular Hair Cell
D018034	3	嗅覚受容神経 Olfactory Receptor Neuron
D010786	3	光受容器 Photoreceptor
D017956	4	無脊椎動物光受容器 Invertebrate Photoreceptor
D020419	4	脊椎動物視細胞 Vertebrate Photoreceptor
D017949	5	錐体 Cone
D017948	5	桿体 Rod
D012374	6	桿体外節 Rod Outer Segment
D012165	4	網膜神経節細胞 Retinal Ganglion Cell
D020671	3	後角細胞 Posterior Horn Cell
D013376	4	膠様質 Substantia Gelatinosa
D012165	3	網膜神経節細胞 Retinal Ganglion Cell
D009476	2	遠心性ニューロン Efferent Neuron
D009046	3	運動ニューロン Motor Neuron
D000870	4	前角細胞 Anterior Horn Cell
D009047	4	ガンマ運動ニューロン Gamma Motor Neuron
D019581	2	ニューロパイル Neuropil
D019600	3	糸屑状構造物 Neuropil Thread
D009562	2	ニッスル小体 Nissl Body
D026602	2	一酸化窒素作動性ニューロン Nitrergic Neuron
D011689	2	プルキンエ細胞 Purkinje Cell
D017966	2	錐体細胞 Pyramidal Cell
D019582	2	老人斑 Senile Plaque
D009490	1	神経分泌系 Neurosecretory System
D003335	2	アラタ体 Corpora Allata
D007030	2	視床下部下垂体系 Hypothalamo-Hypophyseal System
D008473	3	正中隆起 Median Eminence
D010902	3	脳下垂体 Pituitary Gland
D010903	4	脳下垂体前葉 Anterior Pituitary Gland
D052680	5	副腎皮質刺激ホルモン分泌細胞 Corticotroph
D052681	5	性腺刺激ホルモン分泌細胞 Gonadotroph
D052682	5	乳腺刺激ホルモン分泌細胞 Lactotroph
D052683	5	成長ホルモン分泌細胞 Somatotroph
D052684	5	甲状腺刺激ホルモン分泌細胞 Thyrotroph
D052716	4	脳下垂体中葉 Intermediate Pituitary Gland
D052717	5	メラニン細胞刺激ホルモン産生細胞 Melanotroph
D010904	4	脳下垂体後葉 Posterior Pituitary Gland
D010870	2	松果体 Pineal Gland
D013351	2	交連下器官 Subcommissural Organ
D013356	2	脳弓下器官 Subfornical Organ
D017933	1	末梢神経系 Peripheral Nervous System
D001341	2	自律神経系 Autonomic Nervous System
D017776	3	自律神経経路 Autonomic Pathway
D001338	4	自律神経節後線維 Postganglionic Autonomic Fiber
D017777	5	副交感神経節後線維 Postganglionic Parasympathetic Fiber
D017779	5	交感神経節後線維 Postganglionic Sympathetic Fiber
D001339	4	自律神経節前線維 Preganglionic Autonomic Fiber
D002447	4	腹腔神経叢 Celiac Plexus
D007001	4	下腹神経叢 Hypogastric Plexus
D009197	4	筋層間神経叢 Myenteric Plexus
D013153	4	内臓神経 Splanchnic Nerve
D013368	4	粘膜下神経叢 Submucous Plexus
D014630	4	迷走神経 Vagus Nerve
D007823	5	喉頭神経 Laryngeal Nerve
D012009	6	反回神経 Recurrent Laryngeal Nerve
D009620	5	下神経節 Nodose Ganglion
D017615	3	腸管神経系 Enteric Nervous System
D009197	4	筋層間神経叢 Myenteric Plexus
D013368	4	粘膜下神経叢 Submucous Plexus
D005725	3	自律神経節 Autonomic Ganglia
D005726	4	副交感神経節 Parasympathetic Ganglia

ID	Level	Descriptor
D013233	5	星状神経節 Stellate Ganglion
D017783	5	上頚神経節 Superior Cervical Ganglion
D010275	3	副交感神経系 Parasympathetic Nervous System
D005726	4	副交感神経節 Parasympathetic Ganglia
D017777	4	副交感神経節後線維 Postganglionic Parasympathetic Fiber
D014630	4	迷走神経 Vagus Nerve
D007823	5	喉頭神経 Laryngeal Nerve
D012009	6	反回神経 Recurrent Laryngeal Nerve
D009620	5	下神経節 Nodose Ganglion
D013564	3	交感神経系 Sympathetic Nervous System
D005728	4	交感神経節 Sympathetic Ganglia
D013233	5	星状神経節 Stellate Ganglion
D017783	5	上頚神経節 Superior Cervical Ganglion
D013153	4	内臓神経 Splanchnic Nerve
D014666	4	血管運動系 Vasomotor System
D011311	5	圧受容器 Pressoreceptor
D017950	2	感覚神経節 Sensory Ganglia
D005727	3	脊髄神経節 Spinal Ganglion
D005830	3	膝神経節 Geniculate Ganglion
D009620	3	下神経節 Nodose Ganglion
D013136	3	らせん神経節 Spiral Ganglion
D012668	3	三叉神経節 Trigeminal Ganglion
D009411	2	神経終末 Nerve Ending
D009451	3	神経効果器接合部 Neuroeffector Junction
D009469	4	神経筋接合部 Neuromuscular Junction
D009045	5	運動終板 Motor Endplate
D011984	3	感覚受容器 Sensory Receptor
D002628	4	化学受容器 Chemoreceptor
D046569	5	神経上皮細胞 Neuroepithelial Cell
D046568	6	神経上皮小体 Neuroepithelial Body
D018034	5	嗅覚受容神経 Olfactory Receptor Neuron
D010234	5	非クロム親和性傍神経節 Nonchromaffin Paraganglia
D001016	6	大動脈体 Aortic Body
D002344	6	頚動脈小体 Carotid Body
D005924	6	頚静脈小体 Glomus Jugulare
D043485	6	鼓室小体 Glomus Tympanicum
D013650	5	味蕾 Taste Bud
D008465	4	機械受容器 Mechanoreceptor
D006057	5	ゴルジ・マッツォーニ小体 Golgi-Mazzoni Corpuscle
D018862	5	メルケル細胞 Merkel Cell
D009470	5	筋紡錘 Muscle Spindle
D046569	5	神経上皮細胞 Neuroepithelial Cell
D006198	6	聴覚有毛細胞 Auditory Hair Cell
D006199	7	内有毛細胞 Inner Auditory Hair Cell
D018072	7	外有毛細胞 Outer Auditory Hair Cell
D018069	6	前庭有毛細胞 Vestibular Hair Cell
D010141	5	パチーニ小体 Pacinian Corpuscle
D011311	5	圧受容器 Pressoreceptor
D011661	5	肺伸張受容器 Pulmonary Stretch Receptor
D009619	4	侵害受容器 Nociceptor
D010786	4	光受容器 Photoreceptor
D017956	5	無脊椎動物光受容器 Invertebrate Photoreceptor
D020419	5	脊椎動物視細胞 Vertebrate Photoreceptor
D017949	6	錐体 Cone
D017948	6	桿体 Rod
D012374	7	桿体外節 Rod Outer Segment
D013823	4	温度受容器 Thermoreceptor
D010525	2	末梢神経 Peripheral Nerve
D017776	3	自律神経経路 Autonomic Pathway
D001338	4	自律神経節後線維 Postganglionic Autonomic Fiber
D017777	5	副交感神経節後線維 Postganglionic Parasympathetic Fiber
D017779	5	交感神経節後線維 Postganglionic Sympathetic Fiber
D001339	4	自律神経節前線維 Preganglionic Autonomic Fiber
D002447	4	腹腔神経叢 Celiac Plexus
D007001	4	下腹神経叢 Hypogastric Plexus
D009197	4	筋層間神経叢 Myenteric Plexus
D013153	4	内臓神経 Splanchnic Nerve
D013368	4	粘膜下神経叢 Submucous Plexus
D014630	4	迷走神経 Vagus Nerve
D007823	5	喉頭神経 Laryngeal Nerve
D012009	6	反回神経 Recurrent Laryngeal Nerve
D009620	5	下神経節 Nodose Ganglion
D049428	3	血液神経関門 Blood-Nerve Barrier
D003391	3	脳神経 Cranial Nerve
D000010	4	外転神経 Abducens Nerve
D000055	4	副神経 Accessory Nerve
D005154	4	顔面神経 Facial Nerve
D002814	5	鼓索神経 Chorda Tympani Nerve
D005830	5	膝神経節 Geniculate Ganglion
D005930	4	舌咽神経 Glossopharyngeal Nerve
D007002	4	舌下神経 Hypoglossal Nerve
D009802	4	動眼神経 Oculomotor Nerve
D009832	4	嗅神経 Olfactory Nerve
D009900	4	視神経 Optic Nerve
D009897	5	視交叉 Optic Chiasm
D009898	5	視神経円板 Optic Disk
D014276	4	三叉神経 Trigeminal Nerve
D008340	5	下顎神経 Mandibular Nerve
D008036	6	舌神経 Lingual Nerve
D008442	5	上顎神経 Maxillary Nerve
D009882	5	眼神経 Ophthalmic Nerve
D012668	5	三叉神経節 Trigeminal Ganglion
D014321	4	滑車神経 Trochlear Nerve
D014630	4	迷走神経 Vagus Nerve
D007823	5	喉頭神経 Laryngeal Nerve
D012009	6	反回神経 Recurrent Laryngeal Nerve
D009620	5	下神経節 Nodose Ganglion
D000159	4	内耳神経 Vestibulocochlear Nerve
D003056	5	蝸牛神経 Cochlear Nerve
D013136	6	らせん神経節 Spiral Ganglion
D014725	5	前庭神経 Vestibular Nerve
D012583	3	シュワン細胞 Schwann Cell
D009186	4	髄鞘 Myelin Sheath
D009441	5	神経鞘 Neurilemma
D011901	5	ランビエ絞輪 Ranvier's Node
D013127	3	脊髄神経 Spinal Nerve
D008475	5	正中神経 Median Nerve
D009138	5	筋皮神経 Musculocutaneous Nerve
D011826	5	橈骨神経 Radial Nerve
D014459	5	尺骨神経 Ulnar Nerve
D002572	4	頚神経叢 Cervical Plexus
D010791	5	横隔神経 Phrenic Nerve
D008160	4	腰仙骨神経叢 Lumbosacral Plexus
D005267	5	大腿神経 Femoral Nerve
D009776	5	閉鎖神経 Obturator Nerve
D012584	5	坐骨神経 Sciatic Nerve
D010543	6	腓骨神経 Peroneal Nerve
D013979	6	脛骨神経 Tibial Nerve
D013497	7	腓腹神経 Sural Nerve
D013126	4	脊髄神経根 Spinal Nerve Root
D002420	5	馬尾 Cauda Equina
D005727	5	脊髄神経節 Spinal Ganglion
D013900	4	胸神経 Thoracic Nerve
D007367	5	肋間神経 Intercostal Nerve
D013569	1	シナプス Synapse
D054351	2	電気シナプス Electrical Synapse
D009451	2	神経効果器接合部 Neuroeffector Junction
D009469	3	神経筋接合部 Neuromuscular Junction
D009045	4	運動終板 Motor Endplate
D017729	2	シナプス前終末 Presynaptic Terminal
D019599	3	海馬苔状線維 Hippocampal Mossy Fiber
D013570	2	シナプス膜 Synaptic Membrane
D013572	2	シナプス小胞 Synaptic Vesicle
D012679	0	感覚器 Sense Organ
D004423	1	耳 Ear
D004431	2	外耳 External Ear
D054644	3	耳介 Ear Auricle
D004424	3	外耳道 Ear Canal
D004425	3	耳介軟骨 Ear Cartilage
D014432	3	鼓膜 Tympanic Membrane
D004432	2	中耳 Middle Ear
D004429	3	耳小骨 Ear Ossicle
D007188	4	キヌタ骨 Incus
D008307	4	ツチ骨 Malleus
D013199	4	アブミ骨 Stapes
D005064	3	耳管 Eustachian Tube
D043485	3	鼓室小体 Glomus Tympanicum
D013198	3	アブミ骨筋 Stapedius
D013719	3	鼓膜張筋 Tensor Tympani
D007758	2	内耳 Inner Ear
D003051	3	蝸牛 Cochlea
D001489	4	鼓膜基底板 Basilar Membrane
D003052	4	外リンパ管 Cochlear Aqueduct
D003053	4	蝸牛管 Cochlear Duct
D013316	5	血管条 Stria Vascularis
D013680	5	蓋膜 Tectorial Membrane
D009925	4	コルチ器官 Organ of Corti
D006198	5	聴覚有毛細胞 Auditory Hair Cell
D006199	6	内有毛細胞 Inner Auditory Hair Cell
D018072	6	外有毛細胞 Outer Auditory Hair Cell
D007760	5	迷路支持細胞 Labyrinth Supporting Cell
D012405	4	正円窓 Ear Round Window
D012533	4	鼓室階 Scala Tympani
D054738	4	前庭階 Scala Vestibuli
D013136	4	らせん神経節 Spiral Ganglion
D013137	4	らせん板 Spiral Lamina
D012665	3	半規管 Semicircular Canal
D054776	4	半規管 Semicircular Duct
D054777	5	膨大部有毛細胞 Ampulla Hair Cell
D014722	3	前庭迷路 Labyrinth Vestibule
D010046	4	卵円窓 Ear Oval Window
D012444	4	球形嚢と卵形嚢 Saccule and Utricle
D008267	5	聴斑 Acoustic Maculae
D018069	6	前庭有毛細胞 Vestibular Hair Cell
D010037	6	耳石膜 Otolithic Membrane
D014723	4	前庭水管 Vestibular Aqueduct
D004711	5	内リンパ管 Endolymphatic Duct
D004712	6	内リンパ嚢 Endolymphatic Sac
D005123	1	眼 Eye
D000869	2	眼球前部 Anterior Eye Segment
D000867	3	前房 Anterior Chamber
D001082	4	眼房水 Aqueous Humor
D004728	4	角膜内皮 Corneal Endothelium
D002924	3	毛様体 Ciliary Body
D003228	3	結膜 Conjunctiva
D003315	3	角膜 Cornea
D050541	4	ボーマン膜 Bowman Membrane
D003319	4	角膜実質 Corneal Stroma
D003886	4	デスメ膜 Descemet Membrane
D004728	4	角膜内皮 Corneal Endothelium
D019573	4	角膜上皮 Corneal Epithelium
D016850	4	角膜縁 Limbus Corneae
D007498	3	虹彩 Iris
D011680	4	瞳孔 Pupil
D007908	3	水晶体 Crystalline Lens
D007903	4	水晶体嚢胞 Crystalline Lens Capsule
D007904	4	水晶体皮質 Crystalline Lens Cortex
D007907	4	水晶体核 Crystalline Lens Nucleus
D014129	3	線維柱帯網 Trabecular Meshwork
D005143	2	眼瞼 Eyelid
D003228	3	結膜 Conjunctiva
D005140	3	睫毛 Eyelash
D008537	3	マイボーム腺 Meibomian Gland
D007765	2	涙器 Lacrimal Apparatus
D009301	3	鼻涙管 Nasolacrimal Duct
D009801	2	眼球運動筋 Oculomotor Muscle
D010857	2	眼球色素上皮 Pigment Epithelium of Eye
D012160	2	網膜 Retina
D025042	3	アマクリン細胞 Amacrine Cell
D001813	3	血液網膜関門 Blood-Retinal Barrier
D005654	3	眼底 Fundus Oculi
D008266	3	黄斑 Macula Lutea